Evolving force balance during incipient subduction

Michael Gurnis and Chad Hall

Seismological Laboratory, California Institute of Technology, Pasadena, California 91125, USA (gurnis@caltech.edu; chall@gps.caltech.edu)

Luc Lavier

Seismological Laboratory, California Institute of Technology, Pasadena, California 91125, USA

Now at Institute of Geophysics, University of Texas, Austin, Texas 78759–8500, USA (luc@utig.ig.utexas.edu)

[1] Nearly half of all active subduction zones initiated during the Cenozoic. All subduction zones associated with active back arc extension have initiated since the Eocene, hinting that back arc extension may be intimately associated with an interval (several tens of Myr) following subduction initiation. That such a large proportion of subduction zones are young indicates that subduction initiation is a continuous process in which the net resisting force associated with forming a new subduction zone can be overcome during the normal evolution of plates. Subduction initiation is known to have occurred in a variety of tectonic settings: old fracture zones, transform faults, and extinct spreading centers and through polarity reversal behind active subduction zones. Although occurring within different tectonic settings, four known subduction initiation events (Izu-Bonin-Mariana (IBM) along a fracture zone, Tonga-Kermadec along an extinct subduction boundary, New Hebrides within a back arc, and Puysegur-Fiordland along a spreading center) were typified by rapid uplift within the forearc followed by sudden subsidence. Other constraints corroborate the compressive nature of IBM and Tonga-Kermadec during initiation. Using an explicit finite element method within a two-dimensional domain, we explore the evolving force balance during initiation in which elastic flexure, viscous flow, plastic failure, and heat transport are all considered. In order to tie theory with observation, known tectonic settings of subduction initiation are used as initial and boundary conditions. We systematically explore incipient compression of a homogeneous plate, a former spreading center, and a fracture zone. The force balance is typified by a rapid growth in resisting force as the plate begins bending, reaching a maximum value dependent on plate thickness, but typically ranging from 2 to 3×10^{12} N/m for cases that become self-sustaining. This is followed by a drop in stress once a shear zone extends through the plate. The formation of a throughgoing fault is associated with rapid uplift on the hanging wall and subsidence on the footwall. Cumulative convergence, not the rate of convergence, is the dominant control on the force balance. Viscous tractions influence the force balance only if the viscosity of the asthenosphere is $>10^{20}$ Pa s, and then only after plate failure. Following plate failure, buoyancy of the oceanic crust leads to a linear increase with crustal thickness in the work required to initiate subduction. The total work done is also influenced by the rate of lithospheric failure. A self-sustaining subduction zone does not form from a homogeneous plate. A ridge placed under compression localizes subduction initiation, but the resisting ridge push force is not nearly as large as the force required to bend the subducting plate. The large initial bending resistance can be entirely eliminated in ridge models, explaining the propensity for new subduction zones to form through polarity reversals. A fracture zone (FZ) placed in compression leads to subduction initiation with rapid extension of the overriding plate. A FZ must be underthrust by the older plate for ~100–150 km before a transition from forced to self-sustaining states is reached. In FZ models the change in force during transition is reflected by a shift from forearc uplift to subsidence. Subduction initiation is followed by trench retreat and back arc extension. Moderate resisting forces associated with modeled subduction initiation are consistent with the observed youth of Pacific subduction zones. The models provide an explanation for the

compressive state of western Pacific margins before and during subduction initiation, including IBM and Tonga-Kermadec in the Eocene, and the association of active back arcs with young subduction zones. On the basis of our dynamic models and the relative poles of rotation between Pacific and Australia during the Eocene, we predict that the northern segment of the Tonga-Kermadec convergent margin would have initiated earlier with a progressive southern migration of the transition between forced and self-sustaining states.

1. Introduction

[2] Subduction initiation is a vital phase of the plate tectonic cycle. Long-lived and well-developed subduction zones disappear, as the demise of subduction west of the California coast during the Cenozoic shows, and new subduction zones must form. Theoretical studies, as well as interpretation of the Mesozoic and later plate tectonic history of the Pacific, suggest that subduction initiation alters the force balance on plates [*Gurnis et al.*, 2000; *Richards and Lithgow-Bertelloni*, 1996; *Stern and Bloomer*, 1992] and so a detailed picture of subduction initiation is needed if we hope advance our understanding of forces driving and resisting plate motions. Most theoretical studies [*Cloetingh et al.*, 1989; *McKenzie*, 1977; *Mueller and Phillips*, 1991] have concluded that it is difficult to initiate a new subduction zone. Although several studies have examined the initiation of subduction [*Casey and Dewey*, 1984; *Cloetingh et al.*, 1989; *Karig*, 1982; *Kemp and Stevenson*, 1996; *McKenzie*, 1977; *Mueller and Phillips*, 1991; *Stern and Bloomer*, 1992; *Toth and Gurnis*, 1998], the dynamics of this process remain obscure. There remains substantial disagreement and uncertainty about the significance of different processes influencing subduction initiation, the material properties of tectonic plates, and even whether it is possible to initiate a totally new subduction zone in isolation from an existing one.

[3] Subduction initiation refers to the time interval when oceanic lithosphere first descends into the upper mantle. As our models will show, we believe that there are two dynamic states of subduction: forced and self-sustaining. In the first, remote forces from the integrated force from other subduction zones and ridge push, drive the oceanic plate and slab into the upper mantle. Self-sustaining subduction occurs when the negative buoyancy within a subduction zone is sufficiently large to allow subduction to continue while counteracting the resisting forces. A complete understanding of subduction initiation must take into account the evolution from forced to self-sustaining states. There are some models of subduction initiation in which the phase of forced subduction does not exist, such as in the self-nucleation model [e.g., *Stern and Bloomer*, 1992].

[4] The strength of the lithosphere during bending was recognized as potentially the largest resisting component of the development of a new subduction zone [*McKenzie*, 1977]. *McKenzie* [1977] found that an oceanic plate with an initial through-going, dipping fault must be compressed with a stress of at least 80 MPa to overcome the combined influence of elastic plate flexure and frictional resistance across a preexisting fault. *McKenzie* [1977] argued that these conditions are difficult to achieve, consistent with the apparent longevity of trenches in comparison to ridges. Moreover, he suggested that the convergence velocity must be at least 1.3 cm/yr for the thermal anomaly of the slab to persist without diffusing away.

[5] The dynamics of subduction initiation are governed by the interaction of driving and resisting forces, with the balance of forces continuously

evolving during convergence. Forces which resist subduction come from the elastic work needed to bend an initially horizontal plate, frictional resistance at the plate interface, and viscous shear tractions. Forces which drive subduction are the negative buoyancy of the subducting plate and tectonic forces, such as ridge push or slab pull, which may originate far from the nucleating subduction zone. Subduction dynamics are further modulated by geological factors such as preexisting structural heterogeneity and localized density gradients across fracture zones and transform faults. Finally material properties of the plates and underlying mantle may evolve due to the transition of oceanic crust from basalt to eclogite, the release of volatiles during metamorphism, the potential weakening of shear zones with accumulated strain, and the reduction of slab pull due to thermal equilibration. Some geological settings are likely to influence both resisting and driving forces: a spreading ridge placed in compression would likely have thin, weak lithosphere which would allow localization of a new subduction zone, but ridge push forces would oppose convergence. The complex dynamics of such settings are best understood with numerical models.

[6] There are two principle views on the physical mechanism leading to the initiation of subduction. The first and most common is that as the oceanic lithosphere ages and cools, its density increases so that an instability arises and the plate sinks spontaneously in the mantle under its own weight [*Stern and Bloomer*, 1992; *Turcotte et al.*, 1977]. According to the other view, externally applied compressive stresses and moderate convergence are necessary to form a new subduction zone [*McKenzie*, 1977; *Toth and Gurnis*, 1998].

[7] Included in the first view is initiation at a passive continental margin, a model which has received considerable theoretical attention because of the concept of a Wilson cycle (e.g., that ocean basins, such as the Atlantic ocean, periodically close and reopen [*Wilson*, 1966]). Conversely, the goal of this study is to explore potential mechanisms of intraoceanic subduction initiation. In this view, closure of an oceanic basin during a Wilson cycle occurs when intraoceanic subduction zones form within or migrate into Atlantic type basins [*Casey and Dewey*, 1984]. *Cloetingh et al.* [1984, 1989] explored the possibility of a passive margin

plastically failing by means of a sedimentary pile localized atop the oceanic lithosphere at the continent-ocean boundary. They found that it becomes more difficult to cause complete plastic failure of progressively older lithosphere and suggested that if subduction had not initiated by ∼20 Myr after initiating rifting of an Atlantic-type margin, it would only become more difficult with increasing age. *Regenauer-Lieb et al.* [2001] revisited this passive margin scenario and suggested that with a weaker oceanic lithosphere, such as that occurring through the addition of water to olivine [*Hirth and Kohlstedt*, 1996], that a throughgoing shear zone could develop directly on the edge of a 10 km thick sedimentary pile.

[8] The forced convergence hypothesis has received less attention. *Toth and Gurnis* [1998] explored the conditions necessary to initiate subduction within a viscoelastic material with a preexisting dipping fault dissecting the lithosphere. They mapped out the transition between failed and successful subduction initiation regimes for different fault strengths and imposed compressive forces and velocities. They argued that subduction could initiate with ridge push forces if the fault is as weak as a fully developed subduction interface, several MPa. After overcoming the elastic bending force, *Toth and Gurnis* [1998] followed the transition to self-sustaining subduction. As an observational test, they argued that subduction initiation would be accompanied by rapid uplift and then subsidence on the overriding plate near the plate boundary, while the far field would be accompanied by subsidence [e.g., *Gurnis*, 1992].

[9] Most of the modeling approaches used to explore these physical processes are incomplete because they did not simultaneously treat both the elastic bending of the lithosphere, viscous flow in the lithosphere and the mantle in combination with the spontaneous formation of brittle faults and thermal and chemical buoyancy. *Hall et al.* [2003] used a numerical technique that allows for the self-consistent tracking of these processes which we expand upon here. Although a heuristic approach [e.g., *McKenzie*, 1977; *Mueller and Phillips*, 1991] has been of value to determine the relative importance of factors that drive or resist subduction initiation, these approaches provide few tangible predictions. During the initiation of subduction, as we shall demonstrate, the relative and absolute magnitude of the forces

change with time in a manner that is dependent on initial tectonic setting and application of remote forces. As subduction initiation unfolds, the topographic, structural, thermal, and gravitational signals and the stress state of the plate boundary change in space and time. It is through this evolution, and how these observables depend on forces, that hypotheses for subduction initiation must be tested. Numerical methods are essential in order to track the detailed evolution of a nascent subduction zone. Here we use a method which allows us to track the evolution of a viscoelastic plate, fully coupled to the mantle, undergoing elastoplastic deformation, among other processes.

[10] Our study is composed of several parts. We review the geological evidence for subduction initiation so that dynamic models can be formulated and tested. We then systematically study the relevant processes promoting and retarding initiation. Finally, we synthesize these observations and models into an evolutionary framework that will provide a guide to future studies, both observational and theoretical.

2. Observational Record of Subduction Initiation

[11] Since subduction margins are partially consumed and often overprinted by thermal, structural, volcanic, and sedimentary processes, it is generally thought the observational evidence of subduction initiation is limited. However, we show that the record is still of sufficient quality and quantity to allow us to draw first order conclusions on the evolution and dynamics of initiation. There are a range of subduction zones today which have clearly defined beginnings during the Cenozoic (Figure 1). These new subduction zones not only encompassed different tectonic settings during their incipient stage but they are either presently in or span different evolutionary stages from forced to self-sustaining states (Table 1). For example, the Izu-Bonin-Marianas (IBM) subduction zone in the western Pacific is today a mature self-sustaining system but the seafloor of the overriding basins and the island arc volcanics record a clearly defined beginning and subsequent evolution. In contrast, the Fiordland-Puysegur subduction margin on the South Island of New Zealand, again with its inception dated [*House et al.*, 2002], probably has not attained
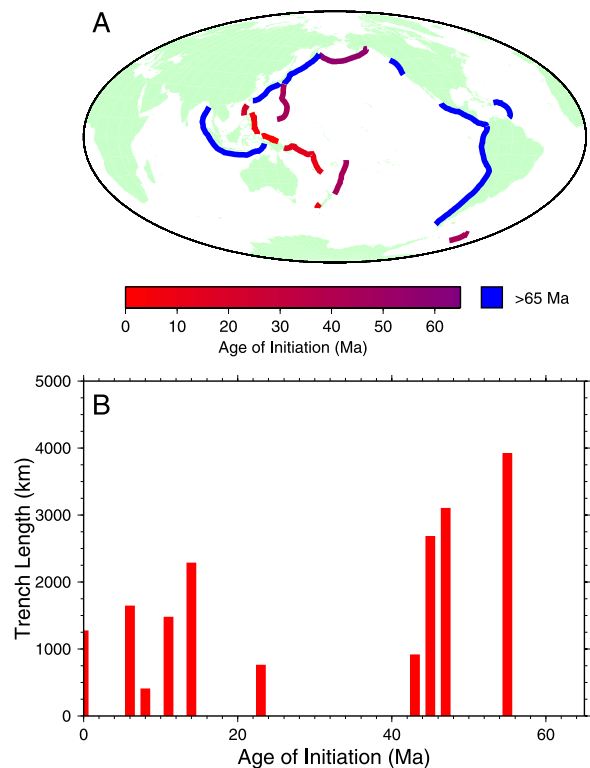

Figure 1. Subduction initiation in the Pacific domain. (a) Position of present-day trenches with age of their initiation color coded. Trenches which initiated before the Late Cretaceous are coded with the same color. (b) Length of present-day trenches versus their age of initiation.

a fully self-sustaining state. In addition, some margins may be incipient subduction zones, but are so young that we do not know if they will evolve into fully fledged subduction zones, such as the Mussau Trench on the eastern boundary of the Caroline plate [*Hegarty et al.*, 1982]. We now distill this observational record of subduction initiation so as to provide tangible constraints for dynamic models. Our discussion is focused on those margins which have constraints on their nucleation, including margins that are self-sustaining, forced, or nascent.

[12] We use two criteria to judge self-sustaining subduction: A total slab length (including Benioff zone and any aseismic portion) that extends through the upper mantle and the presence of back arc spreading. Back arc spreading, as we show, is likely an indication of a slab falling vertically in the mantle after the resisting forces have been overcome [*Hall et al.*, 2003]. If at least one of these

Table 1. Cenozoic Subduction Initiation

Name	Age of Inception, Ma	Present Length, km	Heritage[a]	Current State[b]	Reference
Forced to Self-Sustaining Subduction					
Aleutian	55	3913	FZ	SS	*Scholl et al.* [1986]
Izu-Bonin-Mariana	45	2200	FZ, TF	SS	*Ben-Avraham and Uyeda* [1983]
Tonga-Kermadec	45	2677	Extinct SZ	SS	*Bloomer et al.* [1995]
South Scotia	45	908	SC/TF	SS	*Barker* [2001]
New Britain-San Cristobal	23–5	2278	Reversal	F	*Cooper and Taylor* [1985]
New Hebrides	12–10	1470	Reversal	SS	*Greene et al.* [1994]
Manila	23	755		F	*Yumul et al.* [2003]
Philippine	6	1638		F	*Yumul et al.* [2003]
Puysegur-Fiordland	11–5	400	FZ, SC	F	*Collot et al.* [1995]; *House et al.* [2002]
Hjort	?–0		FZ	F	*Meckel et al.* [2003]
Yap	?–0		SC	F	*Lee* [2004]
Other Potential Incipient Boundaries					
Mussau Trench			TF, FZ	?	*Hegarty et al.* [1982]
Gorringe Bank				F	
Owen Ridge			FZ	F	
Macquarie Seg	0		TZ, SC	F	*Massell et al.* [2000]

[a] Heritage: tectonic setting before subduction. FZ, fracture zone; TF, transform fault; SC, spreading center; reversal: reversal in the polarity of subduction.
[b] Current dynamic state (inferred). SS, self-sustaining; F, forced.

conditions is not met, then the subduction zone is classified as forced.

2.1. Self-Sustaining Subduction Zones

[13] The Izu-Bonin-Marianas, Tonga-Kermadec, Aleutians, New Hebrides, and Scotia subduction zones are all examples of self sustaining subduction, in which the subduction zone is known to have initiated in different tectonic settings within relatively tightly constrained age intervals during the Cenozoic (Figure 1; Table 1).

[14] Izu-Bonin-Mariana is a self-sustaining subduction system as it represents deep mantle penetration of oceanic lithosphere [*Isacks and Molnar*, 1971] which is amongst the oldest [*Müller et al.*, 1997] and potentially most negatively buoyant found. The IBM subduction zone has a distinct beginning in the Middle Eocene [*Bloomer et al.*, 1995], potentially forming as early as 49–48 Ma [*Cosca et al.*, 1998], and a clearly defined subsequent history [*Hussong and Uyeda*, 1981; *Stern and Bloomer*, 1992]. Magnetic lineations of the West Philippine Basin (WPB) show that it is mostly composed of oceanic lithosphere which formed between 60–33 Ma at the now extinct Central Basin Spreading Center (CBSC, Figure 2b) [*Hilde and Lee*, 1984; *Mrozowski et al.*, 1982]. The Kyushu-Palau Ridge (KPR) separates older crust of

the WPB from younger crust which formed during initiation and subsequent back arc extension and arc volcanism of the IBM trench. The perpendicular orientation of the KPR to magnetic lineations formed at the CBSC suggests a ridge-transform intersection [*Uyeda and Ben-Avraham*, 1972]. Despite ambiguities and alternative models [see *Hall*, 2003], *Pearce et al.* [1992] argued that conversion of a transform boundary into an oceanic trench is the simplest explanation for its early history.

[15] The geological evolution of IBM during a 10–15 My interval from ~45 to ~30 Ma, a period of time which *Stern and Bloomer* [1992] referred to as subduction zone infancy, was distinctly different from its subsequent evolution and of other ancient and modern arcs. The early arc was dominated by boninitic volcanism, which requires a high degree of partial melting of a source depleted in major elements but enriched in volatiles, presumably with an abnormally high geothermal gradient [*Pearce et al.*, 1992; *Stern and Bloomer*, 1992]. By palinspastically restoring the Mariana forearc with KPR, *Stern and Bloomer* [1992] found that initial volcanism was exceptionally broad (~200 km) compared to present arcs (~50 km), magma production rates were substantially higher than found in fully developed arcs (with early IBM rates comparable to mid-ocean ridges), and a locally extensional environment.
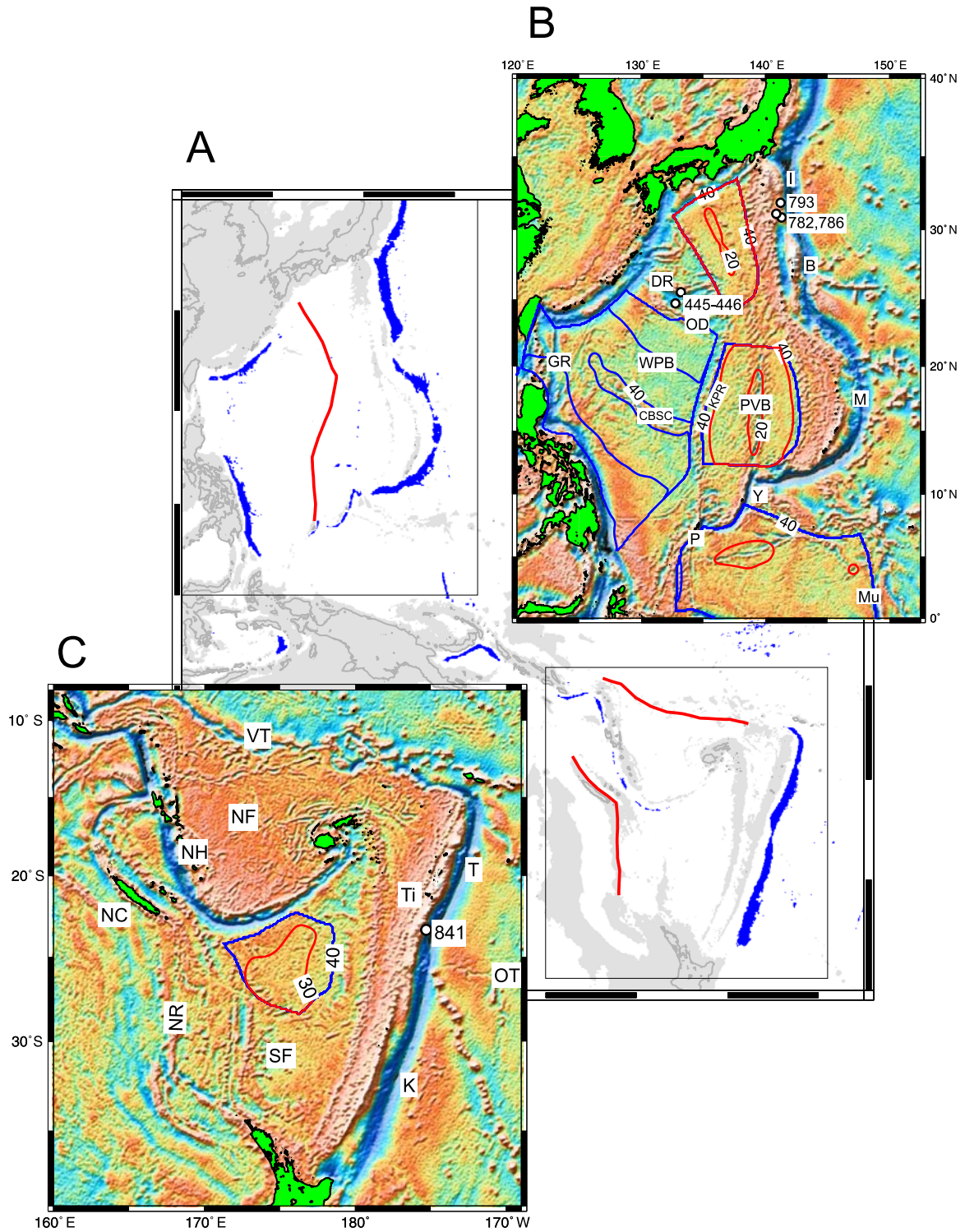
Geochemistry
Geophysics
Geosystems

Figure 2

[16] *Stern and Bloomer* [1992] argue that the IBM tectonic setting was extensional during its infancy. Alternatively, additional evidence suggests that IBM could have been regionally compressive just before becoming locally extensional. Simultaneous with the initiation of IBM subduction, the overriding plates of the West Philippine Basin underwent rapid vertical motions and a fracture zone parallel to the KPR underwent compression. On the WPB, north of the CBSC, there are a set of extinct arcs (Daito Ridge, DR, and Oki Daito Ridge, OD, Figure 2b) which were active in the Mesozoic but subsequently subsided to deep water by the Paleocene [*Mills*, 1980]. Cobbles in an Eocene conglomerate recovered from DSDP hole 446 adjacent to the now flat-topped Daito Ridge show rapid uplift in the Eocene [*Mills*, 1980]. Daito Ridge subsequently subsided to a depth of 1.5 km from the Eocene to Quaternary [*Mizuno et al.*, 1979]. From samples recovered in DSDP hole 445, rapid Eocene uplift and subsidence associated with volcanism, presumably from the adjacent KPR, has been inferred [*Chamley*, 1980]. Rapid uplift is expected where older plates are being under thrust [*Toth and Gurnis*, 1998], such as the rapid uplift synchronous with subduction initiation on the northern MRC [*House et al.*, 2002]. The vertical motions recorded on WPB extinct arcs are consistent with compression preceding subduction initiation, although *Macpherson and Hall* [2001] argue that the uplift was associated with mantle plumes. However, further to the west, on the West Philippine Plate, the Gagua Ridge (GR), another N-S trending fracture zone forming from the CBSC, underwent compression before the middle Eocene (as indicated by a lack of deformation of adjacent flat lying sediments) [*Deschamps et al.*, 1998]. The modern analogue for GR is the Macquarie Ridge Complex (see below), a transpressional margin now undergoing incipient subduction. Since there is only a several million year interval between the formation of the lithosphere at the CBSC and the inferred period of sediment deposition, the compressive stress regime must have relaxed quickly following uplift of the GR. This compression is consistent with our interpretation of the Eocene vertical motions of DR and OD: E-W compression followed by stress relaxation. The near field (<100 km) also shows evidence for vertical motions, potentially related to initiation. During the late Eocene, the frontal arc of Izu-Bonin was within shallow water, as indicated through foraminifers from dredged samples near ODP site 793 (Figure 2b) [*Nishimura*, 1992]. Tectonic subsidence inferred for two drill holes on the outer edge of the forearc (ODP sites 782 and 786, Figure 2b), with controls on paleobathymetry from benthic foraminifers [*Kaiho*, 1992], reveals that the basement subsided by nearly 2 km by the late Eocene and by an additional 1.5 km since [*Bloomer et al.*, 1995]. Forearc subsidence is usually interpreted within the context of "tectonic erosion," although the evidence for this process at the time is ambiguous [*Bloomer et al.*, 1995].

[17] The Tonga-Kermadec subduction zone is presently self-sustaining and also formed at approximately 45 Ma, nearly synchronously with IBM initiation. Evidence on its initiation comes from the drilled Tonga forearc and New Caledonia, which was adjacent to the nucleating margin. Tonga-Kermadec initiated east of the Cenozoic aged North and South Fiji basins (Figure 2c). From the Cretaceous to the Eocene, the region east of Australia, was dominated by rifting, including the opening of the Tasman and Coral Seas [*Gaina et al.*, 1998]. Subduction reinitiated during the Eocene just east of the Norfolk ridge, including the area around New Caledonia. Prior to ~45 Ma, Pacific motion

Figure 2. Maps showing three Pacific subduction zones which initiated during or since the Eocene: Izu-Bonin-Mariana (IBM), Tonga-Kermadec, and the New Hebrides. (a) Base map with trenches shown in blue for depths >6000 m. Heavy red lines are the IBM, Tonga-Kermadec, and New Hebrides incipient margins in their present-day positions. (b) Detail of the IBM trench and back arc regions showing features related to subduction initiation. Labeled features are as follows: I, Izu trench; B, Bonin trench; M, Mariana trench; Y, Yap trench; P, Palau trench; Mu, Mussau trough; WPB, West Philippine Basin; CBCS, Central Basin Spreading Center; DR, Daito Ridge; OD, Oki-Daito Ridge; GR, Gagua Ridge; KPR, Kyushu-Palau Ridge; PVB, Parece Vela Basin. (c) Detail of the Tonga-Kermadec and New Hebrides trenches and back arcs. Labeled features are as follows: T, Tonga Trench; TI, Tongatapu Island; K, Kermadec Trench; OT, Osbourn Trough; NF, North Fiji Basin; SF, South Fiji Basin; NH, New Hebrides Trench and arc; NC, New Caledonia; NR, Norfolk Ridge; VT Vitiaz Trench. Figures 2b and 2c use the following: the red and blue lines are contours of the digital age map from *Müller et al.* [1997]; contour interval is 10 Myr with selected contours marked. Base maps are from *Sandwell and Smith* [1997] satellite-determined free air gravity. Open circles are ODP and DSDP drill holes referred to in the text.

was approximately parallel to the Norfolk ridge while after ~45 Ma it was perpendicular [*Gaina et al.*, 1998]. New Caledonia is dominated by an ophiolite that was emplaced over Mesozoic basement during the Eocene [*Aitchison et al.*, 1995]. Although the Eocene position of the Tonga-Kermadec island arc is uncertain, the thrusting event is thought to mark the resumption of convergence in the southwest Pacific [*Aitchison et al.*, 1995]. A short-lived, northeast verging subduction zone may have occurred from ~50 to ~45 Ma before an opposite polarity WSW verging proto-Tonga system initiated at ~43 Ma [*Eissen et al.*, 1998; *Kroenke*, 1984]. The age of Tonga-Kermadec subduction initiation has been corroborated through study of the Tonga forearc [*Bloomer et al.*, 1995]. The oldest rocks dated in ODP 841 drill hole on the forearc (Figure 2c) cluster around 45 Ma, with the oldest being 46 Ma [*McDougall*, 1994]. A similar age range has been found on 'Eua, an island on the Tonga platform [*Duncan et al.*, 1985].

[18] The kinematics of the motion between the Australian and Pacific plates from ~45 Ma and later is well known from ridge spreading between the two plates at the relative position of the Macquarie Ridge Complex (see below). Since the region between the rifted margin marking the inception of AUS-PAC motion at 45 Ma, the Resolution Ridge margin (RR) and the Norfolk Ridge (NR), has been quiescent since initiation, except for thrusting along NR in response to initiation [e.g., *Symonds et al.*, 1999], we can calculate the relative plate motions during Tonga-Kermadec initiation (Figure 3). Although relative motion between AUS and PAC commenced around 45 Ma [*Keller*, 2003; *Sutherland*, 1995], the first magnetic lineation to appear which is well mapped (18 [*Keller*, 2003]) dates to around 40 Ma [*Cande and Kent*, 1995]. The 40–35 Ma stage pole between the two plates is well constrained [*Keller*, 2003] and shows that 200 to 100 km of convergence must have occurred with southwest verging convergence across New Caledonia (consistent with ophiolite thrusting) and transpression along Norfolk Ridge (Figure 3).

[19] *Bloomer et al.* [1995] assembled a picture of Tonga initiation with similarities and differences from IBM. The original crustal basement for both arcs appear to be missing and *Bloomer et al.* [1995] argue that initial Tonga volcanism may have been broad, although the evidence for this is not yet as compelling as it is for IBM. The initial arc for Tonga was tholeiitic, while IBM was boniniitic and tholeiitic. Compared to IBM where the temperature has been inferred to have been high and partially hydrated beneath the forearc [*Stern and Bloomer*, 1992], the Tonga arc may have had lower temperatures which precluded production of boninites.

[20] Several thousand km of Pacific plate has likely subducted into the mantle since initiation of Tonga-Kermadec. Although a considerable geological record of Pacific plate has been lost since 45 Ma, it is noteworthy that the present orientation of spreading centers and magnetic lineations on the Pacific plate are perpendicular to the strike of the trench, as shown by the extinct Osbourn spreading center, perpendicular to the Tonga trench [*Billen and Stock*, 2000]. The Osbourn is offset by fracture zones which are parallel to the Tonga trench (Figure 2c). The spreading center probably ceased spreading at about 80 Ma. This observation is consistent with N-S fracture zones in the area undergoing E-W convergence during subduction initiation. However, if the Tonga-Kermadec formed on a fracture zone or an old subduction boundary undergoing strike-slip motion during the Eocene, is uncertain.

[21] Initiation of the Aleutian subduction zone dates to the Late Mesozoic to Early Cenozoic (Figure 1). Within the Bering Sea, north-south trending magnetic lineations strike at a high angle to the Aleutian trench and are perpendicular to the trench through much of its length [*Cooper et al.*, 1976]. The lineations are likely Mesozoic in age, inferred as M1 to M13 and having formed on the Kula Plate which has since mostly subducted beneath the Aleutians. *Cooper et al.* [1976] suggests that the Aleutians date to about 80 Ma on the basis of plate motion models and the need to capture the Kula plate with its lineations oriented N-S. Alternatively, *Scholl et al.* [1986] suggested an age of about 55 Ma on the basis of the age of the oldest known arc rocks, which are ≥50 Ma. *Cooper et al.* [1976] and *Scholl et al.* [1986] suggest that the perpendicular orientation of the magnetic lineations to the trench, implies that the subduction zone formed on an old fracture zone, presumably a fracture zone on the Kula plate.

[22] Aleutian initiation must have been different from IBM because of the lack of both boninites during nucleation and subsequent back arc extension. The age of the overriding lithosphere during initiation can be estimated. Since M1 to M13 magnetic lineations range in age from 130–
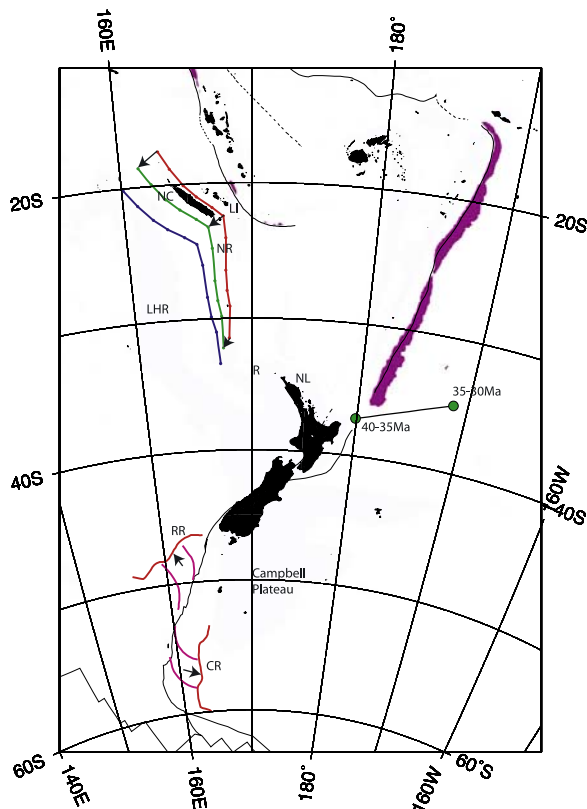
Figure 3. Expected convergence across the line thought to mark Tonga-Kermadec initiation from 40 Ma (red line with small dots) to 35 Ma (green line) and from 35 Ma to 30 Ma (blue) using the stage poles of *Keller* [2003] shown as large green dots. South of the South Island of NZ are the two conjugant rifting margins (Resolution rifted margin, RR, and Campball rifted margin, CR) in red as well as two fracture zones (FZ4 and FZ8) in pink from *Keller* [2003]. Also labeled are Lord Howe Rise (LHR), Norfolk Ridge (NR), New Caledonia (NC), Reinga Ridge (R), Northland (NL), and Loyalty Islands (LI).

120 Ma, the age of the overriding plate would range from either 40–50 Myr (assuming an 80 Ma initiation) or 65–75 Myr (assuming a 55 Ma initiation). These estimates are both considerably larger than the age of the West Philippine Plate during the initiation of IBM which was 0 to about 30 Myr along the strike of the nascent arc.

[23] The New Hebrides subduction zone dates to about 12–10 Ma following a reversal of subduction of the Pacific beneath the Australian plate at the Vitiaz trench (Figure 2c) [*Auzende et al.*, 1988; *Macfarlane et al.*, 1988]. A western belt of volcanic islands along the New Hebrides island arc was active and emergent from 25 Ma to about 14 Ma [*Greene et al.*, 1994; *Macfarlane et al.*, 1988].

Volcanism ceased and the chain became submergent between 14 and 11 Ma, presumably in response to cessation of southwest dipping subduction beneath the Vitiaz Trench [*Macfarlane et al.*, 1988]. At about 10 Ma, the western belt became emergent and by 8 Ma volcanism initiated along the eastern belt. *Macfarlane et al.* [1988] suggests that the uplift of the western belt was the result of a compressive regime associated with initiation of eastern dipping subduction along the New Hebrides Trench. After the initiation of subduction at about 10 Ma, the North Fiji Basin formed by rapid rollback of the New Hebrides Trench [*Auzende et al.*, 1988]. *Greene et al.* [1994] estimate a mean convergence rate between the Australian plate and the western belt of about 13.8 to 14.8 cm/yr during the opening of the North Fiji Basin with most of the convergence due to the motion of the trench to the south west. The oceanic lithosphere which subducted beneath the New Hebrides Trench as well as the plate overlying the nascent subduction zone would be young as there must have been back arc lithosphere where the present North Fiji Basin is today of the same approximate Oligocene age as the South Fiji Basin [e.g., *Taylor and Karner*, 1983].

2.2. Forced Subduction Systems

[24] A number of forced subduction systems in various stages of initiation occur along the Macquarie Ridge Complex (MRC; Figure 4a), south of New Zealand, including the Puysegur-Fiordland subduction zone (Figure 4b). The Puysegur-Fiordland subduction zone forms the northern extremity of the MRC, which itself defines the Australian-Pacific plate margin south of New Zealand. The MRC is clearly expressed in long, narrow bathymetric and gravity highs with adjacent lows from the Hjort Trench in the south to the Puysegur Ridge and Trench in the north [*Hayes and Talwani*, 1972] (Figure 4a). Although clearly juvenile, and potentially not yet internally self-sustaining, Puysegur-Fiordland is a subduction zone: there is Pacific–Australian plate convergence, an oceanic trench (defined gravitationally and bathymetrically), a Benioff zone (with seismicity down to 170 km depth), and sparse, young calc-alkaline volcanism on the overriding Pacific plate [*Davey and Smith*, 1983].

[25] The present plate motion along the Australian-Pacific plate margin (Figures 4a and 4b) is dextral strike-slip with oblique convergence beneath the Puysegur Ridge and Fiordland [*Sutherland*, 1995;
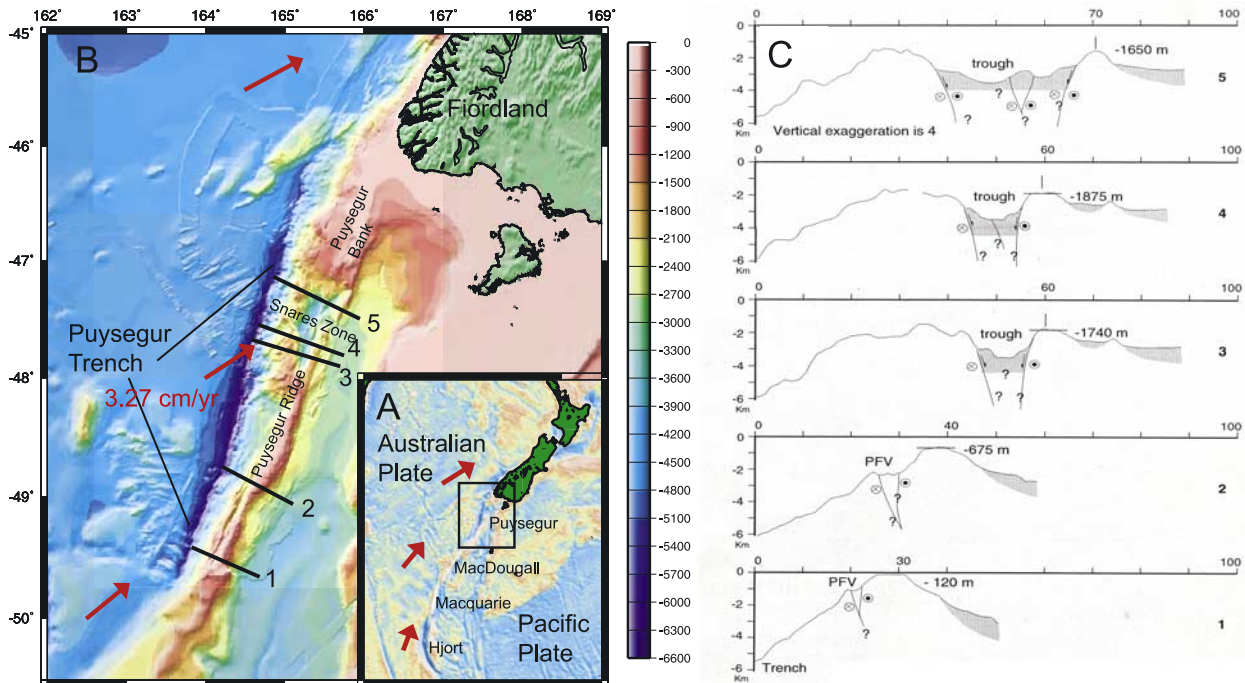
Figure 4. (a) With free-air gravity as a base map [*Sandwell and Smith*, 1997], the Macquarie Ridge Complex (MRC) is shown with the four distinct segments described by *Massell et al.* [2000], Puysegur, McDougall, Macquarie, and Hjort, marked. (b) Detail of the Puysegur multibeam summary over predicted bathymetry. The five labeled black lines are the bathymetric contours shown in Figure 4c. Multibeam bathymetry acquired from 1993 *l'Atalante* Geodynz-sud Leg 2 and augmented by R/V *Ewing* 9513 and by R/VIB *Nathaniel B. Palmer* 9702 is superimposed on the regional bathymetry of New Zealand [*CANZ Group*, 1996]. (c) Bathymetry cross sections and inferred vertical motions on the Puysegur segment (Figure 4c only is from Figure 4 of *Lebrun et al.* [1998] and is reproduced by permission of American Geophysical Union).

Walcott, 1998]. A detailed evolutionary history of the Australia-Pacific margin has been assembled [*Lamarche et al.*, 1997; *Sutherland*, 1995; *Sutherland et al.*, 2000; *Wood et al.*, 1996]. The Tasman Ridge ceased spreading at about 52 Ma and, following a hiatus, a new phase of spreading began along the Australia-Pacific plate margin at about 47 Ma. Rifting here was first orthogonal to the conjugate margins (RR and CR, Figure 3) but became more oblique after ~25 Ma, producing the distinctive curved fracture zones (FZs) that merge with the MRC. After ~10 Ma motion was fully strike-slip with a component of convergence in the Puysegur region.

[26] The curvature of these FZs reflects the southward migration of the AUS-PAC rotation pole during the Miocene [*Sutherland*, 1995; *Walcott*, 1978]. Abyssal hill fabric adjacent to the FZs is clearly visible (Figure 4b) and generally strikes perpendicular to them [*Lamarche et al.*, 1997]; the relationship of this fabric to the MRC varies along strike [*Massell et al.*, 2000].

For example, the McDougall segment (Figure 4a) is mostly parallel to the present plate motion direction and has FZs merging asymptotically with the MRC even on a fine scale, whereas along the Macquarie segment (including Macquarie Island), the FZs are oblique to, and truncated by, the central ridge.

[27] *Massell et al.* [2000] used along-strike variations in FZ orientation and abyssal hill fabric to infer underthrusting of AUS beneath PAC along the Macquarie and Hjort sectors only; these are the two sectors most oblique to modern plate motions. However, there is a distinctive bend in the orientation of the MRC as one moves from the McDougall to the Puysegur segment (Figure 4a), where the modern relative plate motion is also obliquely convergent [*Sutherland et al.*, 2000]. In the Hjort sector, *Meckel et al.* [2003] showed that on the overriding Pacific plate, abyssal hill fabric is perpendicular to the trend of the Hjort Trench. Moreover, they identified curving lineations, sub-parallel to the Hjort

Trench, which they suggested are FZs. Together, these observations suggest that the Hjort Trench nucleated along a preexisting fracture zone.

[28] A well-constrained plate reconstruction of the south Tasman oceanic crust based on fracture zones, magnetic anomalies, DSDP holes, and structures on conjugate rifted margins indicates that 9×10^4 km^2 of Eocene to Miocene aged Australian oceanic plate (~200 km maximum perpendicular to the strike of the margin) was subducted beneath the Pacific Plate along the Puysegur Trench [*Sutherland et al.*, 2000]. Along the Puysegur Ridge, in particular, the morphology of the ridge records a progression from uplift to subsidence at various stages along its length (Figure 4c). The Puysegur ridge consists of discrete flat-topped segments [*Collot et al.*, 1995; *Lebrun et al.*, 1998], the southernmost of which is very close to sea level (−120 m), while to the north along the ridge, the flat tops lie at progressively greater depth (−675 to −1800 m). *Collot et al.* [1995] interpreted the ridge morphology as resulting from subaerial exposure and wave-base erosion implying ~1500 m of subsidence of the ridge following a period of uplift and subaerial exposure and erosion. In addition, the adjacent trench also deepens to the north by ~1 km from −5250 m where the ridge is at sea level to −6250 m where the ridge has subsided by ~1500 m. Simply put, the segment of the ridge which experienced the most convergence has a history of uplift and submergence while the segments that have experienced less convergence show only uplift. The segment of the Puysegur Ridge that has subsided most deeply is referred to as the Snares zone (Figure 4b) [*Lamarche and Lebrun*, 2000].

[29] To the north, Puysegur Ridge merges with Puysegur Bank, an offshore extension of Fiordland with a flat geomorphic surface suggestive of wave erosion. The southern portion of the bank has been imaged seismically, but the erosion surface is tilted and found at 350–800 m depth, suggestive of Quaternary subsidence [*Melhuish et al.*, 1999]. As Puysegur Bank was uplifted, sediments were eroded off the western margin and redeposited on the east, where they were then uplifted by later deformation. The most northerly segment of the incipient subduction zone is the Fiordland region. Using low temperature (U-Th)/He thermochronometry, a regional pattern of Late Cenozoic rock uplift has been revealed in Fiordland [*House et al.*, 2002] consistent with period of intense uplift

between 4 and 10 Ma. *House et al.* [2002] argued that the thermochronometrically deduced crustal thinning, anomalous gravity, and estimates of surface uplift are all consistent with ~2 km of dynamic support.

2.3. Early Stage Systems

[30] There are some incipient margins, all forced, that are so young we do not know if they are going to develop into fully fledged subduction zones, including the Gorringe Bank (N. Atlantic), the Owen Ridge (Arabian Sea) [*Massell et al.*, 2000], the Mussau Trench on the eastern boundary of the Caroline plate [*Hegarty et al.*, 1982], and the Yap Trench on the western boundary of the Caroline plate [*Lee*, 2004].

[31] The Yap Trench (Y, Figure 2b) south of the Marianas may be an example of early stage subduction [*Lee*, 2004]. Although seismically active this system does not have a Benioff zone but has a trench and island arc; the lack of sediments within the trench suggest active subduction today [*Fujiwara et al.*, 2000; *Lee*, 2004]. The Yap is distinctly different from well developed subduction zones with its short trench-arc distance (~50 km) and narrow trench (~50 km) [*Lee*, 2004]. Moreover, neither the island arc nor the inner trench wall are volcanically active, rather they are composed of metamorphic rocks, including ultramafic schists [*Hawkins and Batiza*, 1977]. The arc has a Bouguer gravity high [*Fujiwara et al.*, 2000] compared to a low which usually characterizes fully developed subduction systems (such as the Marianas [*Yang et al.*, 1992]). Metamorphic rocks in the greenschist phase together with the positive gravity anomaly suggest active uplift. Finally, the Yap Trench is perfectly aligned with the extinct spreading center on the East Philippine basin and associated fracture zones (Figure 2b) and supports the hypothesis that new trenches form at preexisting structures [*Lee*, 2004].

[32] The Mussau Trench on the eastern boundary of the Caroline Plate (Figure 2b) is also viewed as juvenile, perhaps only 1 Myr old [*Hegarty et al.*, 1982]. In the southern part of the trench, the trench-ridge morphology (with the trench on the Caroline Plate side) is extremely regular with the overriding plate flexing upward, antisymmetrical to the underthrusting plate flexing downward. The Caroline plate has extinct spreading centers that trend E-W (Figure 2b) and are offset N-S,

presumably by N-S trending FZs. This suggests that the Massau trench nucleated on a preexisting fracture zone. Despite the intriguing juvenile structures on the Caroline plate, the age and timing of the Yap and Massau trenches are poorly known because the convergence history between the Pacific and Caroline plates is difficult to determine [*Lee*, 2001] and the vertical motions have not been dated.

3. Formulation of Numerical Models

[33] During subduction initiation, multiple deformation processes act simultaneously, with conditions varying from elastic plates, to localized plastic shear (brittle failure) in fault zones, to viscous flow in the underlying mantle. To model these multiple deformation processes, we use an explicit finite element code based upon the Fast Lagrangian Analysis of Continua (FLAC) algorithm [*Cundall*, 1989]. Descriptions of the numerical method we use and its application to geophysical problems are given by *Lavier et al.* [2000] and *Poliakov et al.* [1993]. With this method, domains of elastic, plastic, and viscous deformation are determined self-consistently through the temperature, stress, and strain rate dependencies of each process. For example, the coldest portions of the domain are effectively brittle and modeled with a Coulomb elastic-plastic rheology. With the Coulomb rheology, deformation transitions from elastic to plastic when the state of stress exceeds a yield stress

$$\tau = \mu(\sigma_n - P_f) + C, \qquad (1)$$

where μ is the coefficient of friction, $\mu = \tan(\phi)$, σ_n is normal stress, C is cohesion, i.e., the strength of the material at zero normal stress, ϕ is the internal angle of friction, and P_f is pore fluid pressure [*Jaeger and Cook*, 1979]. Where the stress state exceeds the yield envelope, an evolving pattern of faulting approximated by plastic zones is produced by linearly reducing μ and C as a function of plastic strain [*Lavier et al.*, 2000], so that

$$C = C_o + (C_f - C_o) \, \varepsilon_{ps} \big/ \varepsilon_f, \qquad (2)$$

$$\phi = \phi_o + (\phi_f - \phi_o) \, \varepsilon_{ps} \big/ \varepsilon_f, \qquad (3)$$

where the subscripts o and f represent the properties of undeformed and faulted (weakened) materials, ε_{ps} is the accumulated plastic strain, and ε_f is the plastic strain required to fully weaken the material; for plastic strains beyond ε_f, no additional weakening occurs. We chose the initial, undeformed cohesion as $C_o = 44$ MPa and a friction coefficient of $\mu_o = 0.6$, consistent with a normal fault forming at a 60° dip.

[34] For viscoelastic deformation (stresses too low for yielding), the total deviatoric strain rate is described by Maxwell viscoelasticity [*Poliakov et al.*, 1993],

$$\dot{\varepsilon}_{ij} = \frac{1}{2G}\dot{s}_{ij} + \frac{s_{ij}}{2\eta}, \qquad (4)$$

where s_{ij} is the deviatoric stress tensor, G is the shear modulus, and η is the viscosity. The isotropic component of deformation is modeled using the total stress and strain tensors,

$$\varepsilon_{ii} = \frac{\sigma_{ii}}{3K}, \qquad (5)$$

where K is the bulk modulus. Viscous deformation is incompressible and based on non-Newtonian temperature-dependent creep of olivine [*Karato and Wu*, 1993], with viscosity given by

$$\eta = \eta_o \left(\frac{\dot{\varepsilon}_{II}}{\dot{\varepsilon}_o}\right)^{(1/n)-1} \exp\left[\frac{H}{nR}\left(\frac{1}{T} - \frac{1}{T_o}\right)\right], \qquad (6)$$

where $\dot{\varepsilon}_{II}$ is the second invariant of the deviatoric strain rate tensor.

[35] The models are two-dimensional, rectangular domains varying from 400−1000 km wide and 100−300 km deep (Figure 5, Table 2). We use three main types of initially prescribed thermal states, all of which are based on conductively cooling a half-space from above. One initial thermal state mimics homogenous cooling throughout the width of the domain, others model cooling of symmetrically diverging oceanic lithosphere at a mid ocean ridge, while a final set for fracture zones has two homogeneous plates of different thickness abutting one another. The sidewalls are insulating while the top and bottom boundaries are set at a fixed temperatures of 0°C and 1500°C.

[36] The top boundary is a Lagrangian free surface, allowing accurate tracking of topography. The bottom boundary has normal velocities set to zero and tangential velocity left free. On the sidewalls, we prescribed mass conservative velocity boundary
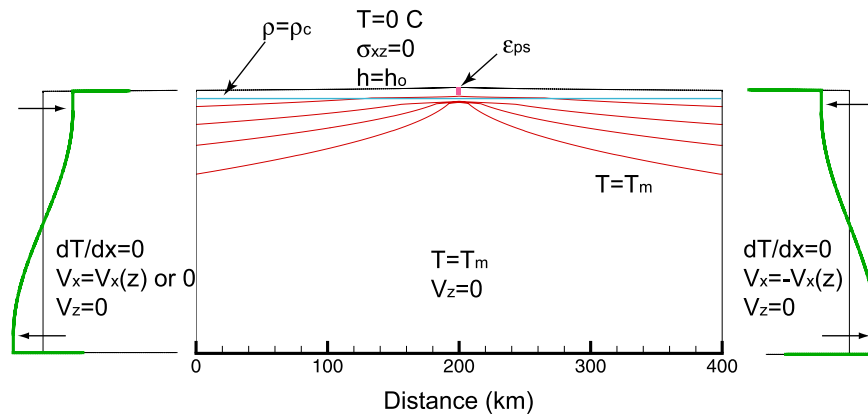
Figure 5. Model setup showing boundary and initial conditions. The initial temperature field is shown with 300°C isotherms in red for Case 15 (as an example). The velocity boundary conditions are shown schematically off to the left and the right of the domain. The depth scale is the same as the horizontal.

conditions. Mass (volume) conservative boundary conditions are essential for the top free surface to give meaningful predictions of topography: net in flow or out flow through the sides would lead to artificial elevation or depression of the free surface. While we could alternatively impose stress boundary conditions on the sides, predetermining a nonzero stress condition that would conserve mass throughout the simulation is a difficult (if not impossible) task.

[37] With imposed velocity boundary conditions on the sidewalls, we interpret the models in terms of the force required to maintain the imposed velocity. The net horizontal force required to maintain the prescribed velocity is determined by integrating the horizontal force on each side. A positive value implies an external force maintains the plate motion, while a negative force implies the imposed velocities are smaller than what would naturally arise from internal forces. We have tracked the force on either side of the domain. The horizontal forces extracted are the sum from pushing from both sides. However, this does not hold after the plate fails because of the inability to transmit stress across the fault zone.

[38] We believe that imposing velocity boundary conditions and extracting the required forces is the most sensible method for understanding subduction initiation. Velocity boundary conditions are the most relevant on the basis of our interpretation of the geological record (see section 2): Subduction initiation occurs only along segments of entire plate boundaries and the forces within the plate boundary only make up a small portion of the total forces available to drive and resist plate motions. The velocity of a plate is expected to be indepen-

dent of the strength of a small segment of that plate's boundary. For example, the initiation of subduction occurring along the Puysegur segment of the MRC (Figure 4) probably only has a small influence on the net force balance of the Australian plate which is influenced by fully developed subduction zones of much greater length and negative buoyancy (Figure 1a). Of course, if the stresses exceed the strength of the plate, then the plate will fail. We track the force on the plate, and not the stress, because the stress is depth dependent and plate thickness varies. Finally, once we have determined the force required to overcome the resisting forces along a particular kind of plate boundary, we can integrate these contributions along strike [*Hall et al.*, 2003].

4. Model Results

4.1. Compression of a Homogeneous Plate

[39] Phenomena associated with incipient subduction are illustrated with a simple model which

Table 2. Model Parameters

Symbol and Definition	Value
C_o initial cohesion	44 MPa
μ_o initial coefficient of friction	0.6
G shear modulus	30 GPa
K bulk modulus	50 GPa
n strain exponent	3.05
$\dot{\varepsilon}_o$ reference strain rate	10^{-15} s^{-1}
η_{max} maximum viscosity	3×10^{27} Pa s
T_{top} top surface temperature	0°C
T_o reference temperature	1400°C
ρ_o reference density	3200 kg m^{-3}
α coefficient of thermal expansion	3×10^{-5} K^{-1}

Table 3. Summary of Cases Studied

Case	Domain, km × km	Initial Thermal State[a]	Vel,[b] cm/yr	Crust	Δx × Δy, km	ε_f	η_o, Pa s	T_m, °C	η_{min}, Pa s	Critical Convergence, km	Critical Work, J/m
1	400 × 200	H, 30 Myr	2 × 0.5	–	0.75 × 0.75	1.0	4.4×10^{18}	1500	10^{20}		
2	400 × 100	H, 30 Myr	2 × 0.5	–	0.75 × 0.75	1.0	4.4×10^{18}	1500	10^{20}		
3	200 × 100	H, 30 Myr	2 × 0.5	–	0.75 × 0.75	1.0	4.4×10^{18}	1500	10^{20}		
4	200 × 100	H, 30 Myr	2 × 0.5	–	.375 × .375	1.0	4.4×10^{18}	1500	10^{20}		
5	400 × 200	H, 30 Myr	2 × 1.0	–	0.75 × 0.75	1.0	4.4×10^{18}	1500	10^{20}		
6	400 × 200	H, 7 Myr	2 × 0.5	–	0.75 × 0.75	1.0	4.4×10^{18}	1500	10^{20}		
7	400 × 200	H, 30 Myr	2 × 0.5	–	0.75 × 0.75	0.25	4.4×10^{18}	1500	10^{20}		
8	400 × 200	H, 30 Myr	2 × 0.5	–	0.75 × 0.75	4.0	4.4×10^{18}	1500	10^{20}		
9	400 × 200	H, 30 Myr	2 × 0.5	–	0.75 × 0.75	∞	4.4×10^{18}	1500	10^{20}		
10	400 × 200	H, 30 Myr	2 × 0.5	–	0.75 × 0.75	1.0	4.4×10^{18}	1500	10^{19}		
11	400 × 200	H, 30 Myr	2 × 0.5	–	0.75 × 0.75	1.0	4.4×10^{18}	1500	10^{21}		
12	400 × 200	H, 7 Myr	2 × 0.5	6 km	0.75 × 0.75	1.0	4.4×10^{18}	1500	10^{20}		
13	400 × 200	H, 7 Myr	2 × 0.5	12 km	0.75 × 0.75	1.0	4.4×10^{18}	1500	10^{20}		
14	400 × 200	RD, 0.5	2 × 0.5	–	0.75 × 0.75	1.0	4.4×10^{18}	1500	10^{20}		
15	400 × 200	RDT, 0.5	2 × 0.5	–	0.75 × 0.75	1.0	4.4×10^{18}	1500	10^{20}		
16	400 × 200	RT, 0.5	2 × 0.5	–	0.75 × 0.75	1.0	4.4×10^{18}	1500	10^{20}		
17	400 × 200	RT, 2.0	2 × 0.5	–	0.75 × 0.75	1.0	4.4×10^{18}	1500	10^{20}		
18	1000 × 300	F, 0, 20	1 × 2.0	–	1.0 × 1.0	0.5	5×10^{19}	1400	10^{18}	107	8.72×10^{16}
19	1000 × 300	F, 0, 40	1 × 2.0	–	1.0 × 1.0	0.5	5×10^{19}	1400	10^{18}	107	1.15×10^{17}
20	1000 × 300	F, 0, 60	1 × 2.0	–	1.0 × 1.0	0.5	5×10^{19}	1400	10^{18}	104	1.29×10^{17}
21	1000 × 300	F, 0, 80	1 × 2.0	–	1.0 × 1.0	0.5	5×10^{19}	1400	10^{18}	100	1.64×10^{17}
22	1000 × 300	F, 10, 20	1 × 2.0	–	1.0 × 1.0	0.5	5×10^{19}	1400	10^{18}	105	9.09×10^{16}
23	1000 × 300	F, 10, 40	1 × 2.0	–	1.0 × 1.0	0.5	5×10^{19}	1400	10^{18}	109	1.17×10^{17}
24	1000 × 300	F, 20, 40	1 × 2.0	–	1.0 × 1.0	0.5	5×10^{19}	1400	10^{18}	130	1.39×10^{17}

[a] Type, value [second value]. H, homogeneous and value is thermal age; R, ridge and value is spreading rate (qualifiers are D for diffuse ridge and T for initial ridge topography); F, fracture zone and values are thermal ages on either side of the fracture zone.
[b] Number of sides pushed on × velocity imposed on each side.

heralds complexities occurring in more realistic scenarios and reinforces earlier results [e.g., *McKenzie*, 1977; *Toth and Gurnis*, 1998]. Case 1 (Table 3) has an initially uniform oceanic lithosphere with an age of 30 Myr, but without a buoyant oceanic crust. The calculation starts with a small anomaly of reduced strength ($\mu = \mu_f$ and $C = C_f$ using $\varepsilon_{ps} = 1$ in equation (2)) at the surface 250 km from the right boundary (Figure 6a). This initial "seed" is incorporated so as to determine the location of the new margin and the polarity of the thrust fault [*Lavier et al.*, 2000]; numerous calculations demonstrate that if there were no seed, a similar shear zone could have nucleated near the edge of the domain or within the lower resolution portions of the mesh due to the explicit nature of the solution, neither of which are desirable. As the lithosphere is compressed from both sides at 0.5 cm/yr a high stress layer, transmitting stress elastically, develops within the top 15 km (Figure 6a). In the presence of a realistic geotherm, deviatoric stress is layered as expected for a Mohr-Coulomb material overlaying a creeping mantle.

[40] From the undeformed state, the total horizontal force rapidly grows in time (Figure 7a) as both the topographic load [*Forsyth*, 1992] from slip on the nucleating plate boundary and elastic plate bending contribute to increasing resistance, which means the force applied to the edges must increase in order to maintain a constant velocity. Simultaneously, plastic strains localize at the initial seed such that a dipping shear zone grows (Figure 6c). The shear zone forms in the first few kilometers of compression and weakening on the fault allows deformation to remain localized. Following this initial phase of localization, the plate thickens, topography grows, and the shear zone penetrates through the elastic layer. Although the plate becomes weaker as the shear zone grows, the bending of the plate dominates the force balance. The stresses that can be supported across the plate boundary are reduced because the shear zone has lost its frictional and cohesive strength. Eventually, the stresses induced across the plate boundary by plate bending, exceed the stress which the fault plane can support. As a result the fault plane yields plastically, topography drops, the plate unbends,
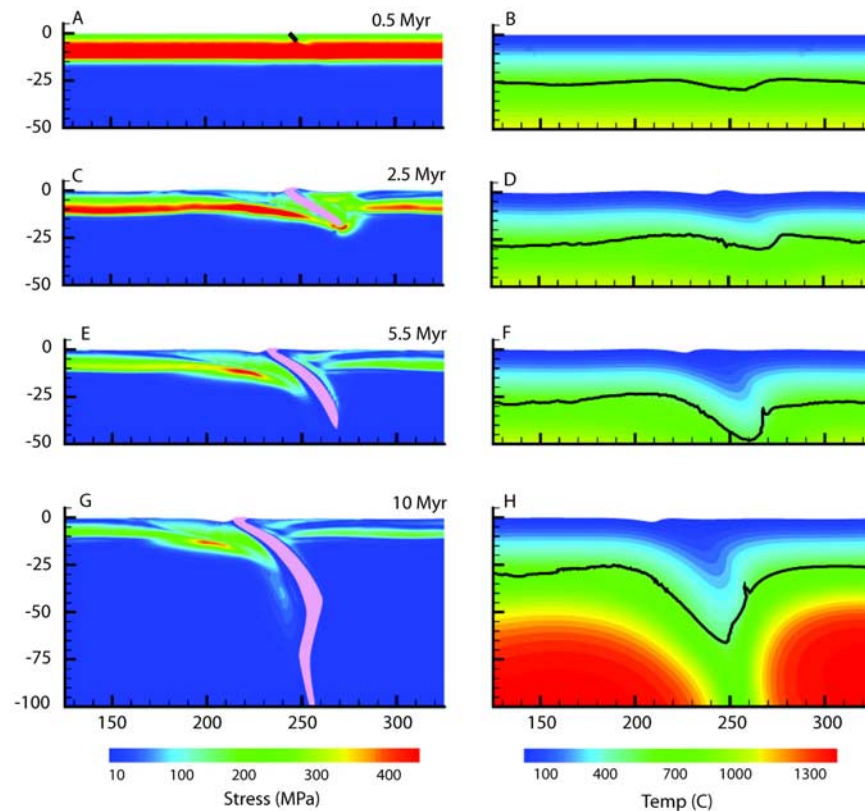
Figure 6. Deformation developing near incipient subduction. Figures 6a, 6c, 6e, and 6g show the cumulative plastic strain (in light purple) overlaying the σ_{II}. In Figure 6a only, the plastic strain is shown in black for clarity (strain 0.2– 1.06), in Figure 6c the strain shown is 2–3.1, in Figure 6e it is 3–5.12, and in Figure 6g it is 3–5.21. For each of the times shown on the left, the temperatures are shown in Figures 6b, 6d, 6f, and 6h with the contour of the effective viscosity for 10^{21} Pa s shown in black.

and the elastic stress within the plate decreases (Figures 6c and 6e). This causes an abrupt drop in F_x between 2 and 2.5 Myr (Figure 7a). After the growth of the shear zone, a trench has developed at the edge of the under thrusting plate and the lower portions of the plate beneath the trench are in compression while the upper parts are in tension (Figure 6c), the normal configuration of a bent plate.

[41] There is a second sudden drop in F_x at 5.5 Myr associated with a rapid contribution of negative buoyancy associated with thickening of the lower lithosphere (Figure 6f). By this time, the shear zone has entirely cut the elastic plate (Figure 6e). A substantial portion of the lower lithosphere is entrained into the down welling (Figure 6h), but this does not develop into a fully self-sustaining system, as evident from the positive force which continues after the sudden drop in F_x at 5.5 Myr for the subducting plate (Figure 7a). Although the topographic expression of this model appears to be similar to a subduction zone, e.g., a realistic looking trench adjacent to a dipping thrust plane,

the vertical velocity of downwelling lower lithosphere is substantially larger than the total convergence velocity (5 cm/yr vertical descent versus 1.0 cm/yr horizontal convergence, at 10 Myr) and the downwelling will eventually detach. Once the plate has been cut by the shear zone, from about 2 Myr onward, the forces on each side that must be applied to compress the lithosphere at a uniform rate become asymmetric, largely because the overriding plate is not being bent and therefore offers little elastic resistance. A finite positive force must be applied to the overriding plate (Figure 7a) as the plate is bent beneath the dipping shear zone. However, the force on the right becomes slightly negative, implying that the plate moves to the left without resistance. This situation is likely facilitated by viscous tractions generated by the downwelling, which also pulls the under thrusting plate downward so that the overriding plate easily moves over the left. The trench migrates to the left with a velocity of about 0.35 cm/yr (Figure 7b), largely accommodating the imposed 0.50 cm/yr velocity of the left plate. The remaining 0.15 cm/yr, if
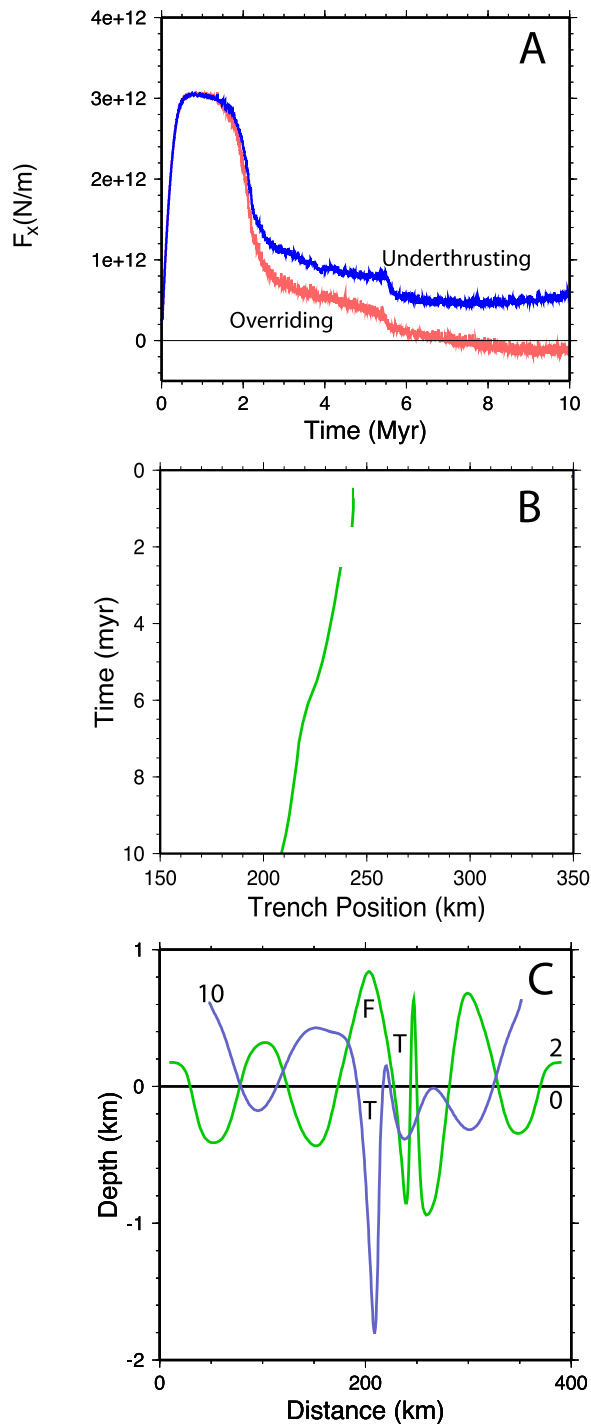
Figure 7. (a) Horizontal force on each side of the domain while a homogeneous oceanic lithosphere is compressed as a function of time. (b) Position of the trench as a function of time. The position of the trench is defined as the minimum in topography and is initially poorly defined while the plate buckles overall. (c) Topography (water loaded) is shown at three different times. The labels are F for fore bulge at 2 Myr and T for trench at 2 and 10 Myr.

distributed evenly over the ~150 km long plate, leads to a small compressive strain rate of ~3 × 10^{-16} s^{-1}.

[42] This is not self-sustaining subduction, as defined above, in that a net external force must be applied to continue to bend the subducting plate (Figure 7a). The deviatoric stress, effective viscosity, and temperature from 5 to 10 Myr demonstrate that despite the asymmetry generated by a dipping zone of low cohesion and friction, and the surface expression of a trench and trench rollback, material is entering the downwelling symmetrically (Figure 6h). The high viscosity of the lower lithosphere continues to couple the cold downwelling to the overriding plate. Since we have asymmetrical convergence at the surface but symmetrical-like convergence at depth, this cannot be a steady configuration.

[43] Before proceeding, several features of the computed force balance are dependent on model geometry and mesh. The duration of the high stress transient depends on the width of the computational domain. Simplifying the problem using a uniform mesh of 750 m in both directions with a box 100 km deep, Case 2 with a width of 400 km is compared with a model half as wide (Case 3). The slope of the initial force-rise doubles in the smaller box, as expected during initial elastic compression (Figure 8a). During the period of high stress the plate undergoes distributed deformation such that the longer box has half the strain rate; this is likely to be at least partly viscous since the deformation is not recovered after the fault forms. Since the fall in the force curve is due to the development of the weak shear zone, the fall only occurs after sufficient strain accumulation near the fault such that the duration is halved for Case 3 from Case 2 when the box width is halved (Figure 8a). In comparison to previous calculations [*Lavier et al.*, 2000], the wide boxes we use lead to substantially larger displacements on the sidewalls prior to plate failure.

[44] As well known, shear zone development is dependent on mesh spacing. For example, comparing Case 3 (with a uniform 750 m mesh) with Case 4 with half the mesh spacing (375 m), the duration before plate failure is halved (Figure 8a), as expected. We find that the weak shear zone width (Δw) during plate failure in the elastic layer is ~2–4 times the mesh spacing [*Lavier et al.*, 2000]. Our results are consistent with the characteristic offset needed across the fault (defined as $\Delta x_c = \varepsilon_f \Delta w$), considering the initial period of distributed strain described above.
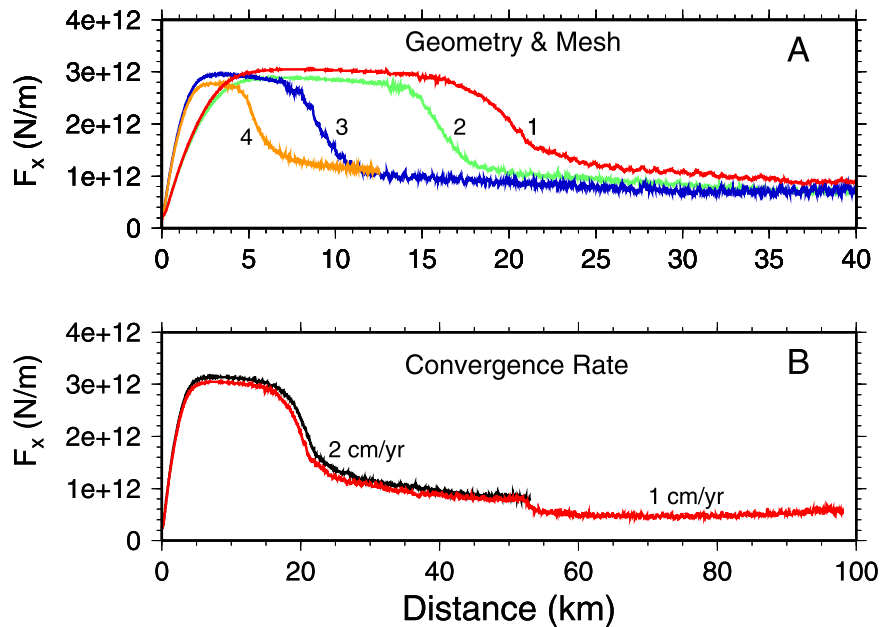
Figure 8. Model comparison in terms of the total force on the left side of the model domain. (a) Influence of geometry and mesh in which Case 1 is compared. Case 2 (green) has a uniform 750 mesh but half the depth of Case 1. Case 3 (blue) has half the width of Case 2, while Case 4 (orange) has half the mesh spacing (375 m) as Case 3. (b) Case 1 with a total convergence rate of 1 cm/yr (red) versus Case 5 (black) with 2 cm/yr.

[45] Initially, homogeneous plates subject to compression typically fail to immediately pass into a fully self-sustaining state, at least for the kinds of (plastic) weakening we have studied. Many of the evolutionary features we have just identified are repeated with varying amplitude and time-scale in other realistic models. We now systematically explore the numerous factors that will alter the force balance and hence will either enhance or inhibit the initiation of subduction.

4.2. Plate Strength and Weakening

[46] The thickness of the plate, governed by its age, is probably the single most important factor influencing the force balance of subduction initiation. For homogeneous elastic plates without weakening and for a brittle layer with little cohesion, the elastic resistance to bending will be approximately proportional to H_e^2, the thickness of the elastic lithosphere [Lavier et al., 2000]. However, growth of regions of plastic failure limits the force which can be attained and this is evident with two cases with weakening. Returning to Case 1, with an age of 30 Myr, H_e, evident as a high stress, near surface layer (Figure 6a), is ~15 km. For 7 Myr lithosphere, this thickness is ~8.5 km. With both friction and cohesion, the force required to cause one plate to underthrust another increases by a

factor of 2.2 as H_e increases (Figure 9a), not 3.1 which would have been expected for lithosphere for no cohesion.

[47] At any instant, the force required for one plate to under-thrust another is proportional to how much the plate has been bent. The strength of the plate is governed by its elastic thickness plus any weakening which subsequently occurs during compression. Conversely, viscous tractions resisting plate motion over the asthenosphere are shown to be negligible from a comparison of Case 1 with 5 with velocities doubled to 1 cm/yr (Table 3, Figure 8b). The area under the curves (the total work done by compression) only deviates slightly, and shows that the force is proportional to the total convergence (i.e., the current elastoplastic state), and not the rate of convergence, similar to viscoelastic models with preexisting faults [Toth and Gurnis, 1998].

[48] The rate of weakening with plate strain is critical for the development of a new subduction zone and if the rate of weakening is not sufficiently fast, no subduction zone will form. For a series of models we have allowed both the internal friction and cohesion of the brittle layer to linearly decrease with increasing plastic strain (equations (2) and (3)), following [Lavier et al., 2000]. If the rate of weakening is sufficiently slow, a buckling instabil-
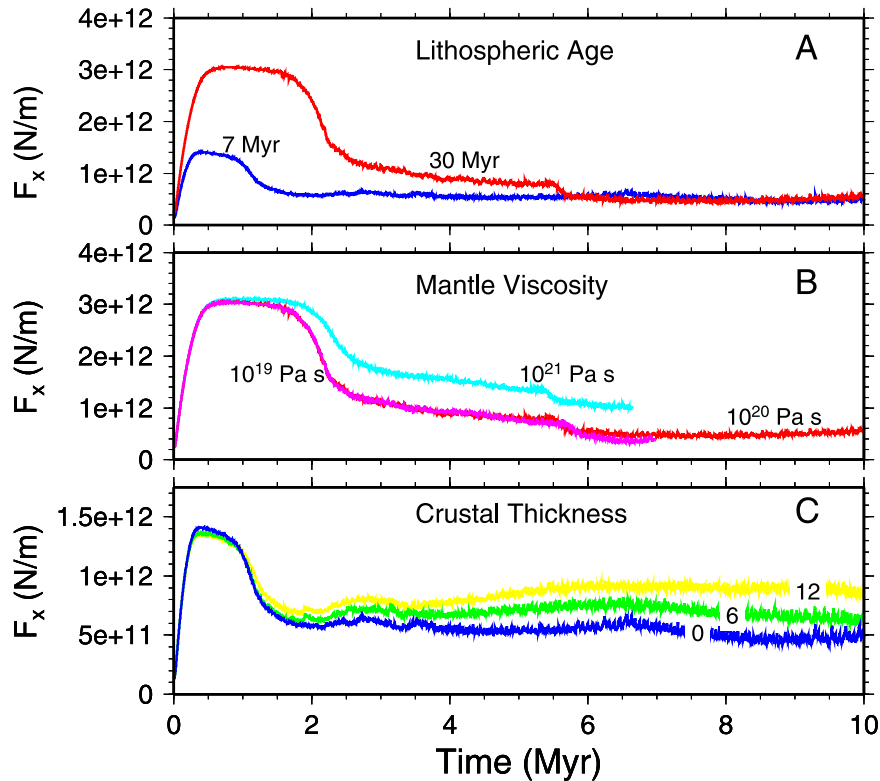
Figure 9. Model comparison in terms of the total force on the left side of the model domain. (a) Case 1 (red) with a thermal age of 30 Myr versus Case 6 (blue) with 7 Myr. (b) Case 7 (blue) with a minimum viscosity of 10^{20} Pa s in the asthenosphere and Case 8 (red) with 10^{19} Pa s. (c) Case 6 (blue) with no crust, Case 9 (green) with a 6 km thick crust, and Case 10 (yellow) with a 12 km thick crust. The density of the crust is 2900 kg/m^3.

ity will grow before compression localizes along the initial weak heterogeneity, while above a threshold a convergent plate margin can grow. The rate of weakening determines how long the system will remain in a phase of high stress (Figure 10). For no weakening, the force attains an asymptotic value determined by the strength envelope and remains there. The time when the force drops from the plateau value depends on the product of the rate of weakening and the mesh size (Figure 10). We have attempted to isolate the critical parameters which determine when the plate breaks by plotting force as a function of displacement near the fault, objectively defined as $\langle \varepsilon \rangle\, 2H_e = 2tV_{bc}H_e/W$ where $\langle \varepsilon \rangle$ is the average strain through the lithosphere, V_{bc} is the total imposed velocity of convergence, and W is box width. In Figure 10 we label each curve with Δx_c defined as $3\,\varepsilon_f\Delta x$ (that is, approximating the width of the shear zone as three time the mesh spacing), demonstrating the cumulative displacement when the stress falls is determined by Δx_c. The peak force is largely independent of the rate of weak-

ening (Δx_c), but the net work required to cause the plate to fail is strongly dependent on Δx_c.

[49] The viscosity of the lithosphere and mantle, particularly the asthenosphere, could influence the force required to initiate subduction, although it is unlikely to be important for Case 1 because the force is independent of the rate of convergence (Figure 8b). To demonstrate this, the minimum viscosity of the system (which occurs within the asthenosphere) is varied for our 30 Myr homogeneous plate case. As expected, the force does not change when the viscosity is reduced to 10^{19} Pa s, but the forces does increase when viscosity is increased to 10^{21} Pa s. Significantly, when the viscosity of the asthenosphere is increased to 10^{21} Pa s (a high oceanic value), the peak force during bending and plate failure are unchanged and viscous tractions only influence the force balance during the longer asymptotic tail after plate failure (Figure 9b).

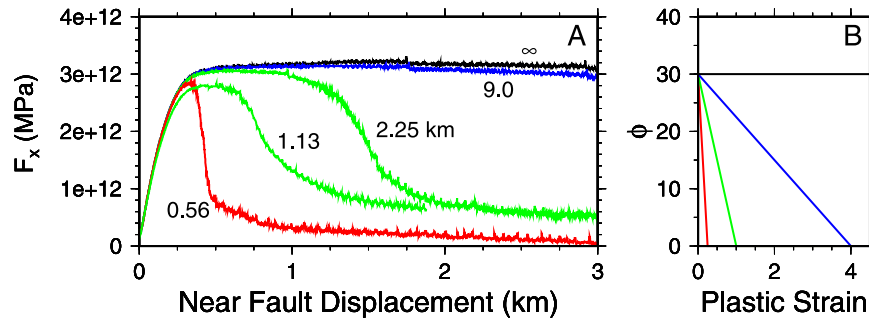[50] There is a compositional buoyancy force associated with oceanic lithosphere, which is less

Figure 10. Force required to compress 30 Myr homogeneous lithosphere for four different rates of weakening. (a) The values labeling each curve is Δx_c, the product of ε_f and the fault width (defined in the text), while the color coding corresponds just to ε_f, the plastic strain when the shear zone has lost all strength (see Figure 10b). The horizontal axis is an objective measure of the displacement near the fault (see text). The duration of the high stress transient is determined by the product of rate of weakening and mesh size. (b) Change in the angle of internal friction as a function of plastic strain for the models shown in Figure 10a.

dense than underlying mantle due to both the density contrast between basaltic crust and peridotitic mantle as well as the depletion in Fe relative to Mg for lithosphere cycled through a ridge melting zone [*Oxburgh and Parmentier*, 1977]. We explore the influence of compositional buoyancy of the crust only, and neglect lithospheric depletion buoyancy. The force required to initiate subduction increases with crustal thickness but this additional force only becomes evident after lateral differences in density at depth develop. Even when we have overestimated this buoyancy, by doubling the thickness of oceanic crust, the force required to compress the lithosphere is not greatly increased in comparison to the peak force required to first bend the lithosphere. However, the excess work done by the compression can exceed the work done during initial plate bending (Figure 9c).

4.3. Initial Tectonic State: Extinct Spreading Center

[51] The factor which most strongly dictates where subduction initiation will occur is the initial tectonic state of the system. The initial tectonic state determines the presence of preexisting strength variations and the distribution of buoyancy forces. The tectonic conditions we have identified as sites of incipient subduction include former spreading centers, fracture zones, passive continental margins, and subduction zones undergoing polarity reversal. We explore the former two types. We have previously presented models of subduction initiation at fracture zones [*Hall et al.*, 2003] and we will further consider this possibility below.

[52] Mid-ocean ridges are an obvious candidate since they may have sufficiently thin lithosphere to allow localization of deformation. Young and thin lithosphere adjacent to ridges could potentially be easily bent under compression. However, a ridge push force will oppose compression and so it is not immediately obvious how easy it is to start a new subduction zone at a former spreading center.

[53] We independently consider factors associated with a ridge so as to isolate how thermal structure and initial topography influence the force balance. A mid-ocean ridge subject to compression is unlikely to have a thermal structure with zero age lithosphere as there will always be some time interval between termination of spreading and initiation of compression. For example, in the case of the northern Macquarie Ridge, this period could be from several million to 10 Myr. We consider a mid-ocean ridge with a thermal structure generated with a 0.5 cm/yr half spreading rate, a small value, but consistent with the slow Miocene spreading rate along the northern MRC. When zero age lithosphere extends to the ridge, we call this an ideal ridge. Moreover, we consider a ridge with a thermal structure reset to a linear geotherm above a depth of 10 km (see Figure 5), referred to as a diffuse ridge, and with no initial topography so as to simulate the effect of a spreading ridge which stopped spreading about 10 Myr ago. Comparing this to an initially homogeneous lithosphere that is everywhere 7 Myr; both models are subject to compression through a 0.5 cm/yr velocity on each side (Figure 11a). In both cases, the initial elastic
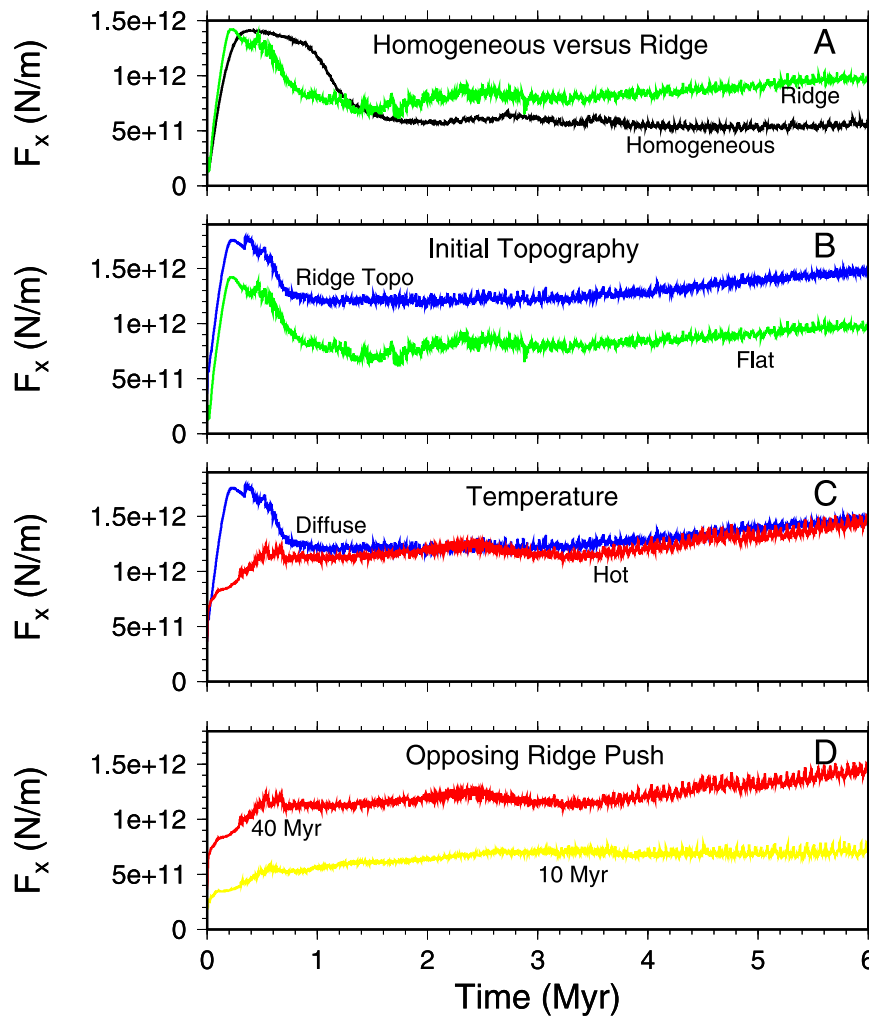
Figure 11. Evolution of force on left plate for models which incorporate different aspects of a mid-ocean ridge. (a) Comparison of a homogeneous, 30 Myr old, plate (black) and mid-ocean ridge (thermally smoothed) and with no initial topography (green). (b) The ridge model in Figure 11a (green) compared with a case in which we add initial topography (blue). (c) Influence of the details of initial ridge thermal structure: diffused (green) and half-space model (red). (d) Changes in the initial age distribution (or opposing ridge push). Age of the plate at the edge of the boxes is indicated.

lithospheres are nearly identical and so are the initial peak stresses (Figure 11a). Although both the homogeneous and ridge cases start with no existing topography, the model with the ridge thermal structure develops 0.7 km of ridge topography by 0.5 Myr by viscous relaxation through the asthenosphere. Plate failure in the diffuse ridge model occurs twice as fast as the homogenous plate (Figure 11a). As expected, the stresses induced across the plate boundary by plate bending exceeds the stress which the fault plane can support. As a result the fault plane yields plastically, topography drops, the plate unbends, and the force decreases suddenly. For the ridge thermal structure, as the two plates continue their convergence,

progressively thicker lithosphere is advected below the dipping fault and after the plate has failed the force curve has a slight positive slope as thicker lithosphere is bent compared to the flatter curve found for the homogeneous plate (Figure 11a).

[54] While holding this "diffuse" ridge thermal structure constant, we compare the initially flat case with one which has initial topography. This initial topography is computed theoretically for a ridge thermal structure assuming the half-space model and a half-spreading rate of 0.5 cm/yr (using equation (4-202) of *Turcotte and Schubert* [1982]) . The initial ridge topography is 2.5 km, considerably larger than that which develops in the initially
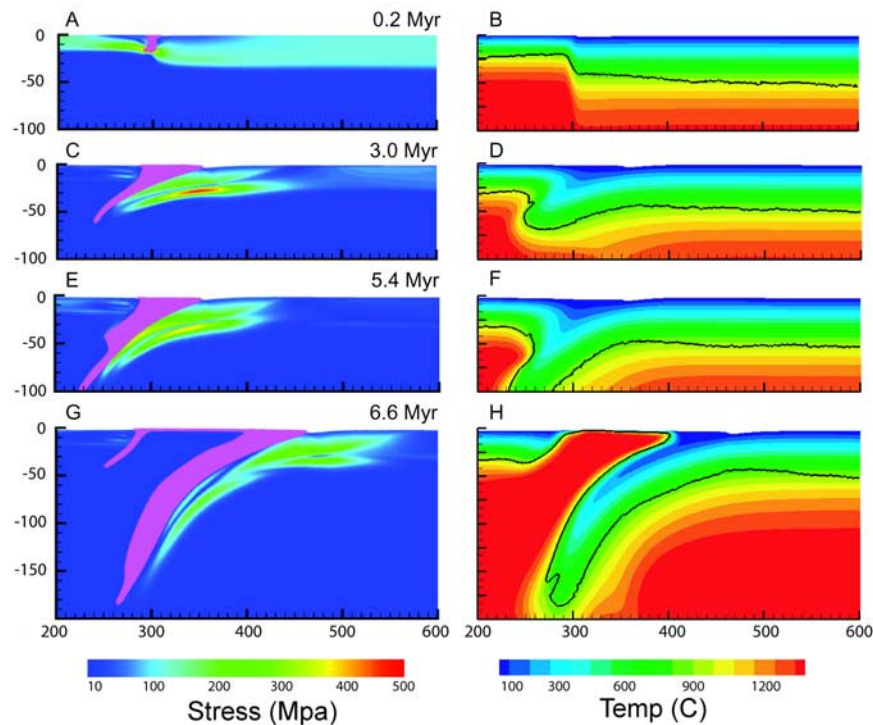
Figure 12. Deformation before and during initiation of a subduction zone at a fracture zone subject to compression. Figures 12a, 12c, 12e, and 12g show the cumulative plastic strain (in light purple) overlaying the σ_{II}. In Figure 12a, strain shown is 0.2–1.0, in Figures 12c it is 1–6.24, in Figure 12e it is 1–6.38, and in Figure 12g it is 1–6.57. For each of the times shown on the left, the temperatures are shown in Figures 12b, 12d, 12f, and 12h with the contour of the effective viscosity shown for 3×10^{21} Pa s shown in black.

flat model by viscous relaxation. The additional topography accounts for an additional $\sim 5 \times 10^{11}$ N/m which must be overcome to compress the plates (Figure 11b).

[55] We consider the influence of initial thermal structure in ridge models with the same initial topography, one having a linear profile in the upper 10 km near the ridge, the other has mantle temperatures reaching the ridge crest. The temperature difference at the ridge influences the early evolution of forces, especially the magnitude of the early peak force (Figure 11c). The entire initial hump in resisting force is eliminated when lithosphere with a typical thermal model of a spreading center is subject to compression. In this case, the initial plate thickness is close to zero at the spreading center, the corresponding small resisting force related to plate bending is therefore immediately dominated by deformation within the growing shear zone. If thickening of the plate were to be faster than the formation of a shear zone the initial increase in force would reappear. For extinct ridges, or ridges which only recently stopped spreading, this is an

approximation because it assumes that spreading stops and convergence starts immediately without any lag. This may be a possible scenario for a back arc environment.

[56] For the model with an ideal ridge thermal structure ("Hot" in Figure 11c) we did not have an initial seed of plastic strain as the thermal structure dictates the location of subsequent deformation. With the diffuse thermal structure, once the elastic plate spanning the former ridge breaks, the force between the two models quickly converges (Figure 11c). Following the convergence of the forces, the force in both models slowly increases due to progressively thicker plates which are pushed below the thrust fault (Figure 11c).

[57] Finally, to isolate the force opposing plate convergence, we increased the spreading rate used to generate the initial conditions from 0.5 cm/yr to 2.0 cm/yr. The ridge push is predicted to increase by a factor of four as the plate age on the side of the box increases to 40 Myr for slower spreading using equation (6-376) of *Turcotte and Schubert* [1982].

However, the force needed to oppose the ridge push and nucleate a new shear zone is smaller than that predicted and only increases by a factor of two.

4.4. Initial Tectonic State: Fracture Zone

[58] Through large gradients in density associated with offsets in plate age [*Stern and Bloomer*, 1992] and extensive serpentinization [*Saleeby*, 1984], it is thought that fracture zones are a preferred initial tectonic condition for subduction initiation. *Hall et al.* [2003], who considered both elastic and viscous forces, demonstrated that elastic bending is too great to be overcome by the initial buoyancy at a fracture zone, even for extremely weak margins. However, if the fracture zone is compressed a new subduction zone could form with a realistic set of parameters. It is this scenario that we further consider here.

[59] For illustration, consider a fracture zone with 10 Myr oceanic lithosphere on one side and 40 Myr on the other subject to a 2 cm/yr compression (Animations 1 and 2; Figure 12). A vertical plane of initial plastic strain is placed at the fracture zone. The initial force peak is as high as that expected for a homogeneous plate, such as the 30 Myr homogeneous lithosphere (3×10^{12} N/m, Case 1; Figure 7). However, the duration of the initial peak in force is reduced to less than 0.5 Myr (Figures 13a and 13b), even though Δx_c is only reduced to 1.5 km from 2.25 km compared to Case 1. Deformation concentrates within the young plate (Figure 12c) and the force is initially close to that expected for the younger plate. The young plate more easily deforms because of the lower yield surface and as the region becomes weaker, deformation becomes localized within the young plate near the original fracture zone. A deep zone of plastic failure extends down to 50 km for the fracture zone case compared to 20 km for the homogeneous plate.

[60] The character of the force curves is contrasted with those for a comparable homogeneous plate (Figure 13a). Following plate failure, the force does not quickly level out as it did for a homogeneous plate, but continues to decrease linearly with time. This linear decrease is due to the buildup of

Figure 13. (a) Forces on the edge of the right plate (with an age 40 Myr) and the left plate (with an age of 10 Myr). (b) Force as a function of compression with a homogenesis plate (with an age of 30 Myr) shown for comparison. (c) Position of the trench as function of time since the inception of convergence.
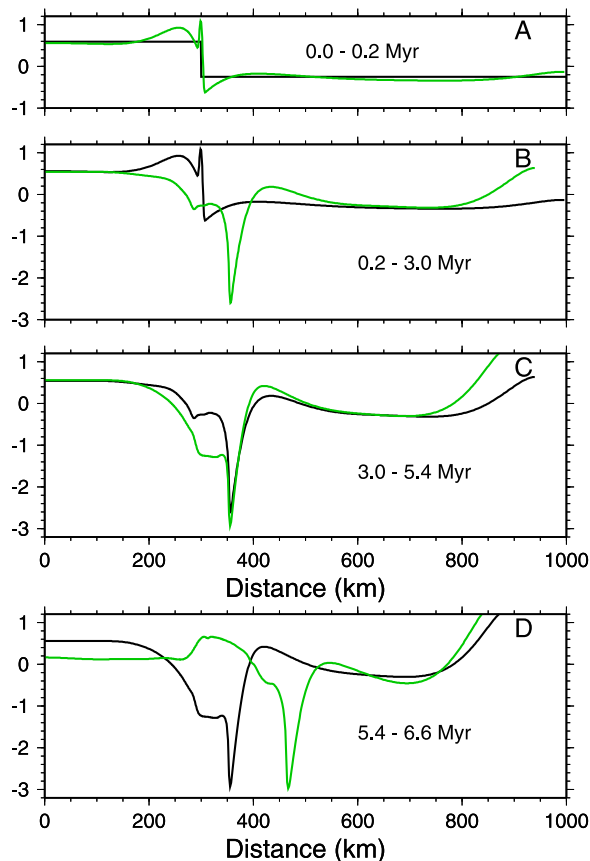
Figure 14. Water loaded bathymetry at various times since the inception of convergence for the model shown in Figures 12 and 13 and Animations 1 and 2. In each frame, topography is shown for the beginning and end of the indicated time periods. The black curve is for the beginning of the interval, while green is for the end.

negative buoyancy (Figures 12d and 12f) as the older plate is thrust beneath the younger. By 2 Myr, the sign of the force on the young plate has reversed substantially, a state which was never found for a homogeneous plate.

[61] The buoyancy force up until 5–6 Myr is not sufficient to overcome the plate bending and so the force on the 40 Myr plate remains positive (Figure 13a). The reversal of forces on the younger plate at 2 Myr occurs as the topographic load developed during coupled convergence subsequently collapses after fault growth and plate decoupling (Figures 12c, 12e, and 14b).

[62] Once the trench forms by ~1 Myr (Figure 14b), its position is relatively stable from 1 to 6 Myr (Figure 13c). By ~6 Myr, a broad zone of plastic failure is located above the negatively buoyant slab (Animation 2; Figure 12e). Suddenly, at ~6 Myr, the underthrusting plate falls vertically (Animation 1).

However, by looking at a slightly earlier time, at ~5.4 Myr, we can see that a positive feedback had set in, feeding off of a small component of vertical motion of the slab. Because of the thermally activated rheology, warm asthenosphere first slowly moves over the slab and into the weak area (Figures 12f and 12h). As the region above the slab becomes weaker, the slab more easily detaches from the overriding plate. As the slab detaches, its vertical descent increases. A broad zone of extension rapidly develops above the slab. During the growth of this instability, the trench rapidly rolls back (Figure 14d) with a velocity of approximately 20 cm/yr (Figure 13c). The final state of the model is clearly one of self sustaining subduction, although the geometry of the domain precludes integrating the model further into the state of self-sustaining subduction.

[63] There are several important features of the topography and its evolution. First, the topography is realistic in terms of trench depth, ~3 km, with a distinct fore bulge (Figures 14b–14d). There is little change in trench depth and width and the forebulge character as it transitions from forced to self-sustaining subduction. However, the forearc topography changes rapidly during this interval. During initial compression, while the force curve grows, the forearc rapidly uplifts (Figure 14a). As the plate relaxes elastically after decoupling, and the buoyancy increases, the forearc subsides by several kilometers (Figures 14b and 14c).

[64] The force required to initiate subduction depends strongly in the age of the oceanic lithosphere on either side of the fracture zone (Figure 15). The maximum resisting force encountered during convergence is sensitive to the age of the overriding plate. Older, thicker, overriding plates require, for constant initial fault dimension, more convergence before establishing a shear zone deep enough to decouple the plates. After the plates are decoupled, however, the force history is largely independent of the overriding plate age [see *Hall et al.*, 2003, Figure 5b]. Therefore, while the maximum resisting force during convergence is most sensitive to the overriding plate age, the age of the subducting plate primarily determines the net work required over the integrated span of convergence to obtain sustained subduction. Two sets of experiments where the subducting plate age is varied for a given overriding plate age (green and red lines, Figure 15) have roughly the same dependence on subducting age (on the basis of the lines being nearly parallel), indicating that the influence of
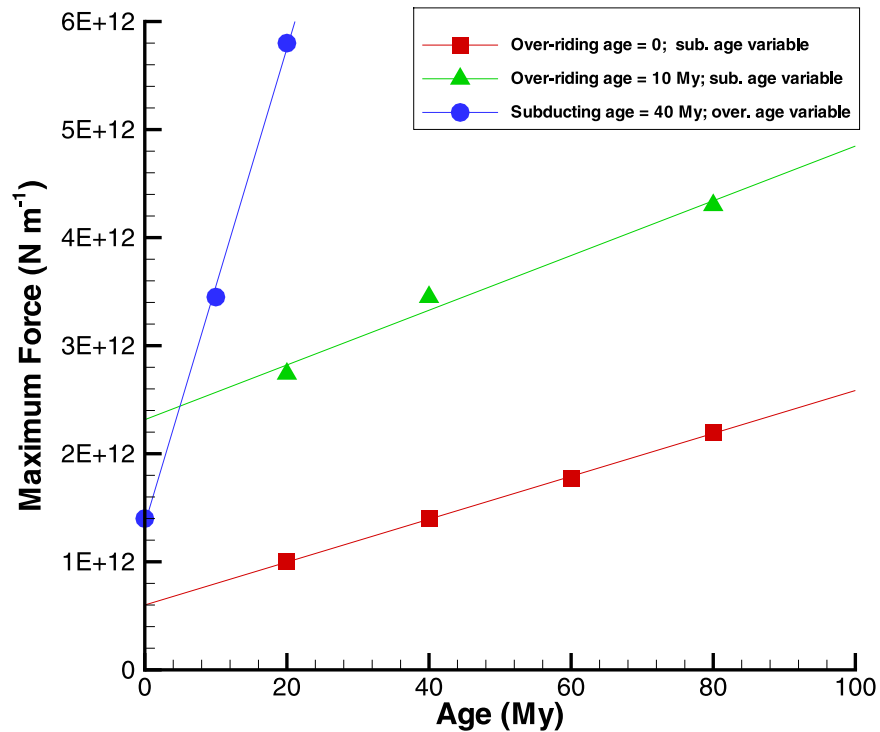
Figure 15. Maximum force achieved versus plate age during the compression of a fracture zone with an associated age difference. For the red squares and green triangles the age of the overriding plate is held constant at 0 Myr and 10 Myr while the age of the subducting plate is varied (as indicated on the horizontal axis). For the blue circles, the age of the subducting plate was held constant at 40 Myr while the age of the overriding was varied, as indicated on the horizontal axis.

subducting versus overriding plate age on the maximum force are largely independent of one another.

[65] Although the total amount of convergence required before subduction initiates is likely a function of age of the two plates, we have found in these models that it is not a sensitive function and only varies between 100 and 130 km (Table 3). We refer to this value as the critical convergence.

5. Discussion and Conclusions

[66] The question of how to initiate a new subduction zone can be answered through a more intimate connection between the geological record of early subduction and dynamic models. Previously, observational and theoretical studies have not been well integrated. In terms of connecting models with the geological record, there are three critical features which must be fulfilled: models need to be tailored to the known initial conditions of nascent subduction; the major inhibiting and driving processes need to be incorporated in a dynamically self-consistent manner; and finally the evolution needs to be tracked from the nascent phase of

nucleation to self-sustaining subduction. We have not been able to achieve these objectives fully, but it is now clear that all three objectives must be achieved. It is essential to consider the initial tectonic state because it invariably has aspects which both facilitate and inhibit subduction to varying degrees (such as an extinct ridge which is a resisting force to convergence through ridge push but is simultaneously a preexisting weak zone which allows localization of deformation). Such tectonic features need to be incorporated as initial and boundary conditions. The latter points together are critical because two forces must initially be overcome to make a subduction zone: fault friction (or growth of a lithosphere-cutting shear zone) and plate bending. Plate bending becomes the principal source of resistance and so models must be followed beyond the simple development of a shear zone and into a true subduction zone with internal forces which can continue to bend the plate.

[67] The initial elastic bending force, per unit length of a nucleating subduction zone (between 10^{12} and 10^{13} N/m) is large, as first pointed out by *McKenzie* [1977], but this result must be reconciled with the ease to which new subduction zones have
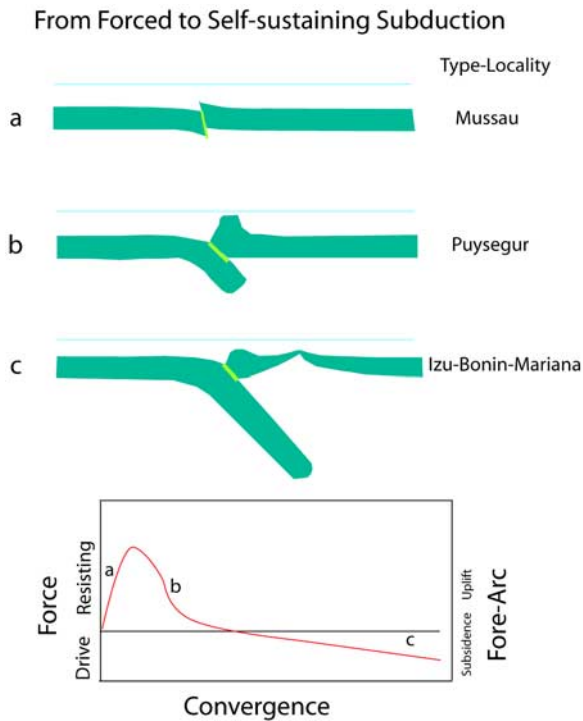
Figure 16. Three phases in the initiation of subduction shown schematically, with type locality and position on the force versus convergence curve indicated.

formed over the Cenozoic. Earlier, this was not necessarily a problem, as *McKenzie* [1977] argued that the major Pacific and Indian oceanic trench systems were thought to be more than 200 Myr old. The geological evidence (geochronological, field mapping, and deep ocean drilling), amassed since shows that three of the major trench systems, Tonga-Kermadec, Izu-Bonin-Marianas, and the Aleutians, are all younger than 80 Myr and perhaps all younger than 55 Myr. Tonga-Kermadec and Izu-Bonin-Mariana both date to about 45 Ma. Moreover, there are a range of even more immature systems. Subduction initiation therefore should not be viewed as a process which is difficult to attain as resisting forces can be overcome during the normal evolution of tectonic plates.

[68] We have attempted to formulate dynamic models to see if the discrepancy between previous ideas and field evidence can be overcome. There is considerable agreement between our dynamic models and nascent to young subduction systems with their initiation phase known from field evidence (e.g., Table 1). The vertical motion of the nascent forearc is a sensitive indicator of the evolving force balance of a nucleating subduction zone (Figure 16).

[69] The match between dynamic models of nucleating a new subduction zone by the convergence at an oceanic fracture zone and evolution of the Izu-Bonin-Mariana subduction system is particularly good, as shown by *Hall et al.* [2003]. Modeled initiation is accompanied by rapid extension of the overriding plate as the older oceanic lithosphere flounders into the upper mantle (and the system transitions from forced to self-sustaining) and explains the catastrophic boninitic Eocene volcanism associated with IBM initiation [*Stern and Bloomer*, 1992]. The principal difference between our numerical model with the conceptual model of *Stern and Bloomer* [1992] is the regional state of stress just as or just before subduction starts to initiate. The immediate tectonic state inferred from the volcanic history and the dynamic models is one of intense local extension; the dynamic models and the *Stern and Bloomer* conceptual model are essentially in agreement. However, *Hall et al.* [2003] interpreted the vertical motion on the overriding plate of the nascent subduction zone from a pair of extinct Mesozoic arcs on the Philippine plate (Daito Ridge and Oki Daito Ridge, Figure 2b) as well as the formation of the Gagua Ridge (Figure 2b) as indicating a state of compression. Having an old overriding plate enhances the likelihood that this plate would first tend to buckle before subduction nucleated while younger lithosphere closer to the CBSC would more easily deform; during the time of IBM nucleation, the extinct ridges would be on >20 Myr old oceanic lithosphere. Moreover, we suggest that the reason that the Gagua Ridge became extinct following compression is that the regional stress regime changed to tensile following the formation of the IBM. We augment this evidence on state of stress with the vertical motion of the Izu-Bonin forearc. During the Eocene the forearc was at shallow water depths (near ODP site 793), which we interpret as resulting from initial compressive uplift. As subduction continued to unfold, however, the forearc (at ODP sites 782 and 786) subsided by nearly 2 km by the Late Eocene (Figure 2b). The opening of the Parece Vela Basin, starting at 26 Ma [*Okino et al.*, 1998], followed the subsidence of the forearc. These vertical motions are consistent with the predictions of compression at a fracture zone which nucleates into a subduction zone (Figures 14a–14c); the dynamic models show ~1 km of uplift followed by ~2–3 km of subsidence over a period of several million years.

[70] Compression is also indicated for the early evolution of the Tonga-Kermadec system. As de-

scribed above, an ophiolite was obducted over Mesozoic basement of New Caledonia during the Eocene [*Aitchison et al.*, 1995]. New Caledonia underwent local uplift and emergence from the early to middle Eocene, but then sank progressively from middle to late Eocene [*Aitchison et al.*, 1995]. This is consistent with the Tonga forearc which was exposed above sea level during the Eocene. A shallow water environment is indicated for the basement of the Tonga forearc [*Hawkins*, 1994]. Detailed study of the subsidence history of ODP 841 suggests that it was just below sea level from 45 to 34 Ma at which point the forearc subsided by approximately 3 km and then by an additional 1–1.5 km [*Clift and MacLeod*, 1999]. A similar subsidence history has been inferred for drill holes on the Tonga platform near Tongatapu Island [*Packham*, 1985]. Like the subsidence inferred for the Izu arc, the Tonga subsidence has been interpreted in terms of tectonic erosion [*Clift and MacLeod*, 1999]. However, given the clearly extensional setting of the forearc and the inferred tensile setting in the past, as well as the seismic uncoupling within both arcs [*Uyeda and Kanamori*, 1979], the tectonic erosion interpretation of subsidence is questionable.

[71] If the vertical motion is a proxy for the state of horizontal stress, then the observation indicates a prolonged state of compression in comparison to IBM. This is consistent with the onset of back arc spreading which only dates to ∼35 Ma within the western part of south Fiji basin [e.g., *Sdrolias et al.*, 2004]. The age of back arc extension apparently only occurs with the change in the state of stress within the forearc. In addition, as described above, the lack of boninitic volcanism during the initiation of the Tonga-Kermadec [e.g., *Bloomer et al.*, 1995] is consistent with a cooler, i.e., older, overriding plate.

[72] The models allow us to address the question as to whether the convergence starting between AUS and PAC at ∼45 Ma (Figure 3) was sufficient to cause subduction to initiate along the Norfolk Ridge. For those models which transition into a self-sustaining state, a convergence which exceeds about 100–130 km must have been attained, e.g., Table 3, Critical Convergence, and *Hall et al.* [2003, Figure 5]. On the basis of the relative poles of *Keller* [2003] this would be achieved within ∼5 Myr in the vicinity of New Caledonia but would have taken longer, ∼10 Ma, at the southerly point of the Norfolk Ridge during times after 45 Ma (Figure 3). A delay in subduction initiation on the

southern parts of the nascent margin is consistent with two sets of observations: The lack of Eocene volcanics in the Kermadec forearc [*Ballance et al.*, 1999] (compared to the Tonga forearc where they appear about the same time as ophiolite emplacement in New Caledonia) and SW verging thrusting along the Reinga Ridge and Northland during the early Miocene [*Herzer et al.*, 1997].

[73] Finally, the initiation of the New Hebrides subduction zone is also associated with uplift of the forearc just prior to rapid back arc opening of the North Fiji Basin. As described above, the western belt of the New Hebrides Island Arc first became emergent and then subsided just before back arc basin extension took place. Again, this is consistent with a reversal in the state of stress from compression to tensional as subduction initiated. For the Aleutian chain, unfortunately, the vertical motion history is unknown during the earliest phases of subduction there and cannot be used as a constraint.

[74] We believe that the substantial back arc basin extension is strongly correlated with young subduction systems and that the most intense phase of back arc extension follows initiation of subduction. This is not to say that back arc extension cannot be associated with mature subduction zones, as the Miocene-Oligocene extension of the Japan Basin [*Taylor and Karner*, 1983] shows. However, there clearly was an intense burst of extension evident in the Parece Vela and Shikoku Basins following initiation of the IBM, South Fiji Basin (and a basin now lost by the subsequent formation of the New Hebrides) following initiation of the Tonga-Kermadec, and North Fiji Basin following the initiation of the New Hebrides subduction zone. The reason for this extension may be related to the ease with which trenches can retreat when slabs first fall through the low viscosity upper mantle; back arc extension may then stop with slowing of retreat when the slabs experience resistance to their descent from the 660 km phase transition and higher viscosities within the lower mantle [*Zhong and Gurnis*, 1995].

[75] For the initiation of subduction at an extinct spreading center, the opposing factors facilitating subduction initiation (through locally thin lithosphere) largely cancel the resistance caused by the opposing ridge push. Subduction would still be more likely to localize and grow at an extinct spreading center than in the midst of a mature, relatively homogeneous plate, despite the resis-

tance caused by an opposing ridge push force (Figure 11).

[76] The rate of weakening with strain of the plate must be sufficiently fast in order for a new subduction zone to develop, and if the rate of weakening is too slow no subduction zone will form. If strain is the principal cause of weakening of the lithosphere in the vicinity of sources of negative buoyancy, then this suggests that plate motion is needed before a new subduction can form.

[77] In our parameterization of fault formation, plastic strain further weakens the site of failure by linearly reducing cohesion and coefficient of friction as strain accumulates (equations (2) and (3)). Models that reach a self-sustained state with less than 200 km of convergence require very low coefficients of friction (<0.02), values much smaller than found experimentally for rocks. Effective coefficients of friction this small likely require the presence of pore fluids at near lithostatic pressures (equation (1)). In this context, the characteristic strain of fault weakening is related to the strain necessary to establish fault-scale fluid ''veins'' or planes. Developing near-lithostatic pore pressures requires that permeability remain below some critical value, with faster dehydration rates increasing this critical value [*Wong et al.*, 1997]. Strain will tend to connect previously isolated pore spaces and decrease the critical permeability. In the context of our parameterized weakening, fault systems that can maintain elevated pore pressure under high strain rates have a low characteristic strain of weakening (fast weakening rate).

[78] Initial asymmetry is important in making the transition from forced to self-sustaining states. Models with asymmetry in the age (thickness) of the two converging plates lead to the development of a much wider weak zone (e.g., Figure 12c) in comparison to a homogeneous plate (e.g., Figure 6c). In such models with asymmetrical plate thickness, the wide weak zone occurs within the thin plate, such that with convergence between the two plates, the weak zone overlies the thicker plate or where the negative buoyancy is localized. This orientation of localized weakness to localized forces primes the system to move into the positive feedback loop described above in which the falling slab allows hot asthenosphere to move upward over the slab. Recent work on the present-day, self-sustaining Tonga-Kermadec system, has shown that a source of weakness above the slab is critical in allowing the system to undergo back

arc extension [*Billen and Gurnis*, 2001; *Billen et al.*, 2003].

[79] Consequently, other mechanisms which allow a region of weakness to develop above the region of plate thickening due to convergence, such as release of volatiles from the subducting slab could be important in allowing the system to transition to the self-sustaining state. This additional source of weakening could control the onset and rate of force reduction (e.g., Figure 10) that must precede the onset of the positive instability causing the rapid back arc opening. The thermal structure resulting from kinematic models has suggested that the volatile release occurs ~10–40 km with the transition of basalt to greenschist and then ecologite [*Peacock*, 1993]. Since the buoyant basaltic crust is an additional resisting force (e.g., Figure 9c), the transition to eclogite and release of volatiles would weaken the region above the slab [*Billen and Gurnis*, 2001; *Hirth and Kohlstedt*, 2003] and may provide an extra localized force and weakness to allow even initially homogeneous plates to make the transition from forced to self-sustaining subduction, because even in our cases with initially homogeneous plates, there is eventual plate thickening (e.g., Figure 6f), but only the lower lithosphere goes unstable. If these weakening processes are sufficiently fast, then the total work expended to transition from forced to self-sustaining states could be reduced significantly, but the peak force required to be overcome is not likely to be greatly influenced (Figure 10).

[80] By our estimations, the Eocene change in Pacific plate motion was sufficient to allow convergence across the Kyushu-Palau Ridge (an intraoceanic fracture zone) and the Norfolk Ridge (an extinct Mesozoic subduction interface) to cause the Izu-Bonin-Mariana and Tonga-Kermadec subduction zones to nucleate and then transition from forced to self-sustaining states. In both cases, the geological evolution of the nascent arc is consistent with an initial compressional environment transitioning to tensile (schematically shown in Figure 16). *Hall et al.* [2003] used a plate reconstruction in which only some of the change in Pacific plate motion evident through the Hawaiian-Emperor chain is due to absolute plate motion (the remaining is due to hot spot motion). This plate model tended to minimize the amount of convergence available to nucleate subduction. Nevertheless, they showed that the force required to initiate IBM subduction ($\sim 2 \times 10^{19}$ N) was substantially smaller than available driving forces (about two orders of magnitude larger). We have

not been able to make a similar estimation for Tonga-Kermadec, but the required forces probably would have been larger than the IBM values because of the stronger overriding plate of the Norfolk Ridge in comparison to the active spreading center of the CBSC (Figure 2b) for IBM. However, because Tonga-Kermadec initiated between the Australian and Pacific plates at a time when we know what the relative motions were between these plates, we have been able to demonstrate that convergence in the vicinity of New Caledonia was more than sufficient to transition the margin from forced to self-sustaining states (~200 km in 5 Myr). This estimate is not subject to the uncertainty associated with the cause of the bend in the Hawaiian-Emperor chain.

Acknowledgments

References

Aitchison, J. C., G. L. Clarke, S. Meffre, and D. Cluzel (1995), Eocene arc-continent collision in New Caledonia and implications for regional southwest Pacific tectonic evolution, *Geology*, *23*, 161–164.

Auzende, J.-M., Y. Lafoy, and B. Marsset (1988), Recent geodynamic evolution of the north Fiji basin (southwest Pacific), *Geology*, *16*, 925–929.

Ballance, P. F., A. G. Ablaev, I. K. Pushchin, S. P. Pletnev, M. G. Birylina, T. Itaya, H. A. Follas, and G. W. Gibson (1999), Morphology and history of the Kermadec trench-arc-backarc basin-remnant arc system at 30 to 32 S: Geophysical profile, microfossil and K-Ar data, *Mar. Geol.*, *159*, 35–62.

Barker, P. F. (2001), Scotia Sea regional tectonic evolution: Implications for mantle flow and palaeocirculation, *Earth Sci. Rev.*, *55*, 1–39.

Ben-Avraham, Z., and S. Uyeda (1983), Entrapment origin of marginal seas, in *Geodynamics of the Western Pacific-Indonesian Region*, *Geodyn. Ser.*, vol. 11, edited by T. W. C. Hilde and S. Uyeda, pp. 91–104, AGU, Washington, D. C.

Billen, M. I., and M. Gurnis (2001), A low viscosity wedge in subduction zones, *Earth Planet. Sci. Lett.*, *193*, 227–236.

Billen, M. I., and J. Stock (2000), Origin and morphology of the Osbourn Trough, *J. Geophys. Res.*, *105*, 13,481–13,489.

Billen, M. I., M. Gurnis, and M. Simons (2003), Multiscale dynamics of the Tonga-Kermadec subduction zone, *Geophys. J. Int.*, *153*, 359–388.

Bloomer, S. H., B. Taylor, C. J. MacLeod, R. J. Stern, P. Fryer, J. W. Hawkins, and L. Johnson (1995), Early arc volcanism and the ophiolite problem: A perspective from drilling in the western Pacific, in *Active Margins and Marginal Basins of the Western Pacific*, *Geophys. Monogr. Ser.*, vol. 88, edited by B. Taylor and J. Natland, pp. 1–30, AGU, Washington, D. C.

Cande, S. C., and D. V. Kent (1995), Revised calibration of the geomagnetic polarity timescale for the Late Cretaceous and Cenozoic, *J. Geophys. Res.*, *100*, 6093–6095.

CANZ Group (1996), *Undersea New Zealand*, Natl. Inst. of Water and Atmos. Res., Wellington, New Zealand.

Casey, J. F., and J. F. Dewey (1984), Initiation of subduction zones along transform and accreting plate boundaries, triple junction evolution, and forearc spreading centres—Implications for ophiolitic geology and obduction, in *Ophiolites and Oceanic Lithosphere*, edited by I. G. Gass, S. J. Lippard, and A. W. Shelton, *Geol. Soc. Spec. Publ.*, *13*, 269–290.

Chamley, H. (1980), Clay sedimentation and paleoenvironment in the area of Daito Ridge (Northwest Philippine Sea) since the Early Eocene, *Initial Rep. Deep Sea Drill. Proj.*, *58*, 683–693.

Clift, P. D., and C. J. MacLeod (1999), Slow rates of subduction erosion estimated from subsidence and tilting of the Tonga forearc, *Geology*, *27*, 411–414.

Cloetingh, S. A. P. L., M. J. R. Wortel, and N. J. Vlaar (1984), Passive margin evolution, initiation of subduction and the Wilson cycle, *Tectonophsyics*, *109*, 147–163.

Cloetingh, S., R. Wortel, and N. J. Vlaar (1989), On the initiation of Subduction zones, *Pure Appl. Geophys.*, *129*, 7–25.

Collot, J.-Y., G. Lamerche, R. A. Wood, J. Delteil, M. Sosson, J.-F. Lebrun, and M. F. Coffin (1995), Morphostructure of an incipient subduction zone along a transform plate boundary: Puysegur ridge and trench, *Geology*, *23*, 519–522.

Cooper, A. K., D. W. Scholl, and M. S. Marlow (1976), Plate tectonic model for the evolution of the eastern Bering Sea Basin, *Geol. Soc. Am. Bull.*, *87*, 1119–1126.

Cooper, P. A., and B. Taylor (1985), Polarity reversal in the Solomon Islands arc, *Nature*, *314*, 428–430.

Cosca, M. A., R. J. Arculus, J. A. Pearce, and J. G. Mitchell (1998), 40Ar/39Ar and K-Ar geochronological age constraints for the inception and early evolution of the Izu-Bonin-Mariana arc system, *Island Arc*, *7*, 579–595.

Cundall, P. A. (1989), Numerical experiments on localization in frictional materials, *Ingenieur Archiv.*, *58*, 148–159.

Davey, F. J., and E. G. C. Smith (1983), The tectonic setting of the Fiordland region south-west New Zealand, *Geophys. J. R. Astron. Soc.*, *72*, 23–38.

Deschamps, A. E., S. E. Lallemand, and J. Y. Collot (1998), A detailed study of the Gagua Ridge: A fracture zone uplifted during a plate reorganization in the Mid-Eocene, *Mar. Geophys. Res.*, *20*, 403–423.

Duncan, R. A., T. L. Vallier, and D. A. Falvey (1985), Volcanic episodes at 'Eua, Tonga Islands, in *Geology and Offshore Resources of Pacific Island Arcs—Tonga Region*, *Circum-Pac. Counc. Energy Miner. Resour. Earth Sci. Ser.*, edited by D. W. Scholl and T. L. Vallier, pp. 281–290, Circum-Pac. Counc. for Energy and Miner. Resour., Houston, Tex.

Eissen, J.-P., A. J. Crawford, J. Cotten, S. Meffre, H. Bellon, and M. Delaune (1998), Geochemistry and tectonic significance of basalts in the Poya Terrane, New Caledonia, *Tectonophysics*, *284*, 203–219.

Forsyth, D. W. (1992), Finite extension and low-angle normal faulting, *Geology, 20*, 27–30.

Fujiwara, T., C. Tamura, A. Nishizawa, K. Fujioka, K. Kobayashi, and Y. Iwabuchi (2000), Morphology and tectonics of the Yap trench, *Mar. Geophys. Res.*, *21*, 69–86.

Gaina, C., R. D. Müller, J.-Y. Royer, J. Stock, J. Hardebeck, and P. Symonds (1998), The tectonic history of the Tasman Sea: A puzzle with 13 pieces, *J. Geophys. Res.*, *103*, 12,413–12,433.

Greene, H. G., J. Y. Collot, M. A. Fisher, and A. J. Crawford (1994), Neogene tectonic evolution of the New Hebrides island arc: A review incorporating ODP drilling results, *Proc. Ocean Drill. Program Sci. Results*, *134*, 19–46.

Gurnis, M. (1992), Rapid continental subsidence following the initiation and evolution of subduction, *Science*, *255*, 1556–1558.

Gurnis, M., S. Zhong, and J. Toth (2000), On the competing roles of fault reactivation and brittle failure in generating plate tectonics from mantle convection, in *The History and Dynamics of Global Plate Motions*, *Geophys. Monogr. Ser.*, vol. 121, edited by M. A. Richards, R. Gordon, and R. van der Hilst, pp. 73–94, AGU, Washington, D. C.

Hall, C., M. Gurnis, M. Sdrolias, L. L. Lavier, and R. D. Müller (2003), Catastrophic initiation of subduction following forced convergence across fracture zones, *Earth Planet. Sci. Lett.*, *212*, 15–30.

Hall, R. (2003), Cenozoic geological and plate tectonic evolution of SE Asia and the SW Pacific: Computer-based reconstructions, model and animations, *J. Asian Earth Sci.*, *20*(4), 353–431.

Hawkins, J. (1994), Petrologic synthesis: Lau Basin Transect (Leg 135), *Proc. Ocean Drill. Program Sci. Results*, edited by J. Hawkins, L. Parson, and J. Allan, *135*, 879–905.

Hawkins, J., and R. Batiza (1977), Metamorphic rocks of the Yap Arc-Trench system, *Earth Planet. Sci. Lett.*, *37*, 216–229.

Hayes, D. E., and M. Talwani (1972), Geophysical investigations of the Macquarie Ridge complex, in *Antarctic Oceanology II: The Australian-New Zealand Sector*, *Anatrct. Res. Ser.*, vol. 19, edited by D. E. Hayes, pp. 211–234, AGU, Washington, D. C.

Hegarty, K. A., J. K. Weissel, and D. E. Hayes (1982), Convergence at the Caroline-Pacific Plate boundary: Collision and subduction, in *The Tectonic and Geological Evolution of Southeast Asian Seas and Islands, Part 2*, *Geophys. Monogr. Ser.*, vol. 27, edited by D. E. Hayes, pp. 326–348, AGU, Washington, D. C.

Herzer, R. H., et al. (1997), Seismic stratigraphy and structural history of the Reinga Basin and its margins, southern Norfolk Ridge system, *N. Z. J. Geol. Geophys.*, *40*, 425–451.

Hilde, T. W. C., and C.-S. Lee (1984), Origin and evolution of the west Philippine Basin: A new interpretation, *Tectonophysics*, *102*, 85–104.

Hirth, G., and D. L. Kohlstedt (1996), Water in the oceanic upper mantle: Implications for rheology, melt extraction and the evolution of the lithosphere, *Earth Planet. Sci. Lett.*, *144*, 93–108.

Hirth, G., and D. Kohlstedt (2003), Rheology of the upper mantle and the mantle wedge: A view from the experimentalists, in *Inside the Subduction Factory*, *Geophys. Monogr. Ser.*, vol. 138, edited by J. Eiler, pp. 83–105, AGU, Washington, D. C.

House, M. A., M. Gurnis, P. J. J. Kamp, and R. Sutherland (2002), Uplift in the Fiordland region, New Zealand: Implications for incipient subduction, *Science*, *297*, 2038–2041.

Hussong, D. M., and S. Uyeda (1981), Tectonic processes and the history of the Mariana arc: A synthesis of the results of Deep Sea Drilling Project Leg 60, in *Initial Rep. Deep. Sea Drill. Proj.*, *60*, 909–929.

Isacks, B., and P. Molnar (1971), Distribution of stresses in the descending lithosphere from a global survey of focal-mechanism solutions of mantle earthquakes, *Rev. Geophys.*, *9*, 103–174.

Jaeger, J. C., and N. G. W. Cook (1979), *Fundamentals of Rock Mechanics*, John Wiley, Hoboken, N. J.

Kaiho, K. (1992), Eocene to Quaternary benthic foraminifers and paleobathymetry of the Izu-Bonin arc, Legs 125 and 126, *Proc. Ocean Drill. Program Sci. Results*, *126*, 285–310.

Karato, S.-I., and P. Wu (1993), Rheology of the upper mantle: A synthesis, *Science*, *260*, 771–778.

Karig, D. E. (1982), Initiation of subduction zones: Implications for arc evolution and ophiolite development, in *Trench-Forearc Geology: Sedimentation and Tectonics on Modern and Ancient Active Plate Margins*, edited by J. K. Leggett, *Geol. Soc. Spec. Publ.*, *10*, 563–576.

Keller, W. R. (2003), Cenozoic plate tectonic reconstructions and plate boundary processes in the Southwest Pacific, Ph.D. thesis, Calif. Inst. of Technol., Pasadena.

Kemp, D. V., and D. J. Stevenson (1996), A tensile flexural model for the initiation of subduction, *Geophys. J. Int.*, *125*, 73–94.

Kroenke, L. W. (1984), *Cenozoic Tectonic Development of the Southwest Pacific*, 123 pp., *Tech. Bull. 6*, U.N. Econ. Soc. Comm. Asia Pac., Comm. Co-ord. Jt. Prospect Miner. Resour. South Pac. Offshore Areas, New York.

Lamarche, G., and J.-F. Lebrun (2000), Transition from strike-slip faulting to oblique subduction: Active tectonics at the Puysegur margin, south New Zealand, *Tectonophsyics*, *316*, 67–89.

Lamarche, G., J.-Y. Collot, R. A. Wood, M. Sosson, R. Sutherland, and J. Delteil (1997), The Oligocene-Miocene Pacific-Australia plate boundary, south of New Zealand: Evolution from oceanic spreading to strike-slip faulting, *Earth Planet. Sci. Lett.*, *148*, 129–139.

Lavier, L. L., W. R. Buck, and A. N. B. Poliakov (2000), Factors controlling normal fault offset in an ideal brittle layer, *J. Geophys. Res.*, *105*, 23,431–23,442.

Lebrun, J.-F., G. D. Karner, and J.-Y. Collot (1998), Fracture zone subduction and reactivation across the Puysegur ridge/trench system, southern New Zealand, *J. Geophys. Res.*, *103*, 7293–7313.

Lee, S.-M. (2001), From spreading and transform fault to subduction: Examples from the boundaries of the Caroline Plate, *Eos Trans. AGU*, *82*(47), Fall Meet. Suppl., Abstract T42G-04.

Lee, S.-M. (2004), Deformation from the convergence of oceanic lithosphere into Yap Trench and its implications for early stage subduction, *J. Geodyn.*, *37*, 83–102.

Macfarlane, A., J. N. Carney, A. J. Crawford, and H. G. Greene (1988), Vanuatu—A review of the onshore geology, in *Geology and Offshore Resources of Pacific Island Arcs—Vanuatu Region*, *Circum-Pac. Counc. Energy Miner. Resour. Earth Sci. Ser.*, edited by H. G. Greene and F. L. Wong, pp. 45–91, Circum-Pac. Counc. for Energy and Miner. Resour., Houston, Tex.

Macpherson, C. G., and R. Hall (2001), Tectonic setting of Eocene boninite magmatism in the Izu-Bonin-Mariana forearc, *Earth Planet. Sci. Lett.*, *186*, 215–230.

Massell, C., M. F. Coffin, P. Mann, S. Mosher, C. Frohlich, C. S. Duncan, G. Karner, D. Ramsay, and J.-F. Lebrun (2000), Neotectonics of the Macquarie Ridge Complex, Australia-Pacific plate boundary, *J. Geophys. Res.*, *105*, 13,457–13,480.

McDougall, I. (1994), Dating of rhyolitic glass in the Tonga forearc (Hole 841B), *Proc. Ocean Drill. Program, Sci. Results*, *135*, 923.

McKenzie, D. P. (1977), The initiation of trenches: A finite amplitude instability, in *Island Arcs, Deep Sea Trenches and Back-Arc Basins*, *Maurice Ewing Ser.*, vol. 1, edited by M. Talwani and W. C. Pitman, pp. 57–61, AGU, Washington, D. C.

Meckel, T. A., M. F. Coffin, S. Mosher, P. Symonds, G. Bernardel, and P. Mann (2003), Underthrusting at the Hjort Trench, Australian-Pacific plate boundary: Incipient subduction?, *Geochem. Geophys. Geosyst.*, *4*(12), 1099, doi:10.1029/2002GC000498.

Melhuish, A., R. Sutherland, F. J. Davey, and G. Lamarche (1999), Crustal structure and neotectonics of the Puysegur oblique subduction zone, New Zealand, *Tectonophysics*, *313*, 335–362.

Mills, W. (1980), Analysis of conglomerates and associated sedimentary rocks of the Daito Ridge, Deep Sea Drilling Project Site 445, *Initial Rep. Deep Sea Drill. Proj.*, *58*, 643–657.

Mizuno, A., Y. Okuda, S. Niagumo, H. Kagami, and N. Nasu (1979), Subsidence of the Daito Ridge and associated basins, North Philippine Sea, in *Geophysical and Geological Investigations of Continental Margins*, edited by J. S. Watkins, L. Montadert, and P. W. Dickerson, Am. Assoc. of Pet. Geol, Tulsa, Okla.

Mrozowski, C. L., S. D. Lewis, and D. E. Hayes (1982), Complexities in the tectonic evolution of the West Philippine Basin, *Tectonophysics*, *82*, 1–24.

Mueller, S., and R. J. Phillips (1991), On the initiation of subduction, *J. Geophys. Res.*, *96*, 651–665.

Müller, R. D., U. R. Roest, J.-Y. Royer, L. M. Gahagan, and J. G. Sclater (1997), Digital isochrons of the world's ocean floor, *J. Geophys. Res.*, *102*, 3211–3214.

Nishimura, A. (1992), Carbonate bioclasts of shallow-water origin at Site 793, *Proc. Ocean Drill. Program, Sci. Results*, *126*, 231–234.

Okino, K., S. Kasuga, and Y. Ohara (1998), A new scenario of the Parece Vela Basin genesis, *Mar. Geophys. Res.*, *20*, 21–40.

Oxburgh, E. R., and E. M. Parmentier (1977), Compositional and density stratification in oceanic lithosphere: Causes and consequences, *J. Geol. Soc. London*, *133*, 343–355.

Packham, G. H. (1985), Vertical tectonics of the Tonga ridge from the Tongatapu oil exploration wells, in *Geology and Offshore Resources of Pacific Island Arcs—Tonga Region*, *Circum-Pac. Counc. Energy Miner. Resour. Earth Sci. Ser.*, edited by D. W. Scholl and T. L. Vallier, pp. 291–300, Circum-Pac. Counc. for Energy and Miner. Resour., Houston, Tex.

Peacock, S. M. (1993), The importance of blueschist to eclogite dehydration reactions in subducting oceanic crust, *Geol. Soc. Am. Bull.*, *105*, 684–694.

Pearce, J. A., S. R. van der Laan, R. J. Arculus, B. J. Murton, T. Ishii, D. W. Peate, and I. J. Parkinson (1992), Bonnite and harzburgite from Leg 125 (Bonin-Mariana Morearc): A zcase study of magma genesis during the initial stages of subduction, *Proc. Ocean Drill. Program, Sci. Results*, *125*, 623–659.

Poliakov, A. N. B., Y. Podladchikov, and C. Talbot (1993), Initiation of salt diapirs with frictional overburdens: Numerical experiments, *Tectonophsyics*, *228*, 199–210.

Regenauer-Lieb, K., D. A. Yuen, and J. Branlund (2001), The initiation of subduction: Criticality by addition of water?, *Science*, *294*, 578–580.

Richards, M. A., and C. Lithgow-Bertelloni (1996), Plate motion changes, the Hawaiian-Emperor bend, and the

apparent success and failure of geodynamic models, *Earth Planet. Sci. Lett.*, *137*, 19–27.

Saleeby, J. B. (1984), Tectonic significance of serpentinite mobility and ophiolitic melange, *Geol. Soc. Am. Spec. Pap.*, *198*, 153–168.

Sandwell, D. T., and W. H. F. Smith (1997), Marine gravity anomaly from ERS-1, Geosat and satellite altimetry, *J. Geophys. Res.*, *102*, 10,039–10,045.

Scholl, D. W., T. L. Vallier, and A. J. Stevenson (1986), Terrane accretion, production, and continental growth: A perspective based on the origin and tectonic fate of the Aleutian-Bering Sea region, *Geology*, *14*, 43–47.

Sdrolias, M., R. D. Müller, A. Mauffret, G. Bernardel, and P. A. Symonds (2004), Enigmatic formation of the Norfolk Basin, SW Pacific: A plume influence on back-arc extension, *Geochem. Geophys. Geosyst.*, *5*, Q06005, doi:10.1029/2003GC000643.

Stern, R. J., and S. H. Bloomer (1992), Subduction zone infancy: Examples from the Eocene Izu-Bonin-Mariana and Jurassic California arcs, *Geol. Soc. Am. Bull.*, *104*, 1621–1636.

Sutherland, R. (1995), The Australia-Pacific boundary and Cenozoic plate motions in the SW Pacific: Some constraints from Geosat data, *Tectonics*, *14*, 819–831.

Sutherland, R., F. Davey, and J. Beavan (2000), Plate boundary deformation in South Island, New Zealand, is related to inherited lithospheric structure, *Earth Planet. Sci. Lett.*, *177*, 141–151.

Symonds, P., H. Stagg, and I. Borissova (1999), The transition from rifting and break-up to convergence in the Lord Howe Rise-Norfolk Ridge region, in *Mid-Cretaceous to Recent Plate Boundary Processes in the Southwest Pacific*, edited by M. Hough, pp. 94–95, Geol. Soc. Am., Boulder, Colo.

Taylor, B., and G. D. Karner (1983), On the evolution of marginal basins, *Rev. Geophys.*, *21*, 1727–1741.

Toth, J., and M. Gurnis (1998), Dynamics of subduction initiation at preexisting fault zones, *J. Geophys. Res.*, *103*, 18,053–18,067.

Turcotte, D. L., and G. Schubert (1982), *Geodynamics*, John Wiley, Hoboken, N. J.

Turcotte, D. L., W. F. Haxby, and J. R. Ockendon (1977), Lithospheric instabilities, in *Island Arcs, Deep Sea Trenches, and Back-Arc Basins*, *Maurice Ewing Ser.*, vol. 1, edited by M. Talwani and W. C. Pitman, pp. 63–69, AGU, Washington, D. C.

Uyeda, S., and Z. Ben-Avraham (1972), Origin and development of the Philippine Sea, *Nature Phys. Sci.*, *240*, 176–178.

Uyeda, S., and H. Kanamori (1979), Back-arc opening and the mode of subduction, *J. Geophys. Res.*, *84*, 1049–1061.

Walcott, R. I. (1978), Present tectonics and Late Cenozoic evolution of New Zealand, *Geophys. J. R. Astron. Soc.*, *52*, 137–164.

Walcott, R. I. (1998), Modes of oblique compression: Late Cenozoic tectonics of the South Island of New Zealand, *Rev. Geophys.*, *36*, 1–26.

Wilson, J. T. (1966), Did the Atlantic close and then re-open?, *Nature*, *211*, 676–681.

Wong, T.-f., S.-c. Ko, and D. L. Olgaard (1997), Generation and maintenance of pore pressure excess in a dehydrating system: 2. Theoretical analysis, *J. Geophys. Res.*, *102*, 841–852.

Wood, R., G. Lamarche, R. Herzer, J. Delteil, and B. Davy (1996), Paleogene seafloor spreading in the southwest Tasman Sea, *Tectonics*, *15*, 966–975.

Yang, C. S., J. Segawa, and Y. Fukuda (1992), Density structure of the Mariana Arc and its vicinity obtained from successive inversion of the gravity anomaly, *Tectonophsyics*, *206*, 325–339.

Yumul, G. P., C. B. Dimalanta, R. A. Tamayo, and R. C. Maury (2003), Collision, subduction and accretion events in the Philippines: A synthesis, *Island Arc*, *12*, 77–91.

Zhong, S., and M. Gurnis (1995), Mantle convection with plates and mobile, faulted plate margins, *Science*, *267*, 838–843.